

CHAPTER 1

INTRODUCTION

1.1 General statement

Peridot is a mineral, and minerals are naturally occurring inorganic crystalline elements or compounds having definite physical and chemical composition and when used for beauty, are termed as gemstones. Gemstones occur worldwide but rare. These form by surface water, igneous hydrothermal activity, metamorphism, as mantle material and concentration through action of water (Keller, 1990). Many other materials, which do not satisfy the norms of the gemstones, e.g., opal, agate, fluorite, jade, malachite, lapis lazuli, jasper and pearl, also come in gemstone category.

In Pakistan, many gemstones including ruby, spinel, pargasite, emerald, aquamarine, topaz, tourmaline, peridot, garnet, bastnasite, epidote, quartz, moonstone etc are found (e.g. Kazmi and O'Donoghue, 1990; Khan and Kausar, 2010). These are mineralized in the suture zone between the Indian plate and Kohistan island arc-back arc terrane. Aquamarine, tourmaline, quartz and moonstone occur in pegmatites and ruby in marble in the Gilgit-Baltistan region. Hydrothermally formed gemstones include pink topaz in Katlang, Mardan and bastnasite in the Warsak area of KPK province.

Peridot was discovered in Pakistan in 1994 (<http://semiprecious.com>) and mined at an altitude ~4000 m above sea level in the Nanga Parbat region of the Himalayan mountain ranges. Since then, this area has been investigated thoroughly (e.g. Jan et al., 1993; Jan and Khan, 1996; Kausar and Khan, 1996; Hussain, 2005; Bouilhol et al., 2009; Khan and Kausar, 2010).

Peridot is also reported from Hawaii, Arizona, Zabargat, Island or St. John Island in the Red Sea where the country rock is serpentinitized dunite and in basalts of the Ross Island, Antarctica. Myanmar, Australia, Brazil, China, Mexico and Norway are also known for the peridot occurrences.

Jan and Khan (1996) studied the crystal forms of the peridots showing prominent prisms (100) and (110), basal pinacoid (001), and pyramidal (021) and (111) faces.

According to them, the faces of peridot lack overgrowths and in few cases, the prismatic faces possess striations and pits elongated to the c-axis. A few pyramidal faces are also pitted. Antigorites occupies the pits.

Peridot of the Sapat area is light yellow to green to deep yellow green with different shades and transparent to translucent. Glass-like fractures are present in it. The hardness ranges from 6.5 to 7. The specific gravity, refractive indices and birefringence range up to 3.26-3.44; (α) 1.644-1.653 and γ 1.682-1.689) and 0.033 to 0.038 respectively (Jan and Khan, 1996). These values resemble those of the two samples studied by Koivula et al. (1994) who also reported other optical determinations, such as, UV fluorescence.

It is to be noted that peridot is a gemstone name for dark green variety of olivine with general formula of R_2SiO_4 (where R" represents Mg, Fe^{2+} , Mn and Ca). It is a solid solution between Mg and Fe end members such as forsterite (Mg_2SiO_4) and fayalite (Fe_2SiO_4). The specific gravity, refractive indices and other physical properties vary with variation in the chemistry. The forsterite (Fo) ranges in composition from $\sim Fo_{87}$ to Fo_{97} . The color of peridot depends on its iron content. Samples with high forsterite content (Fo_{95}) and low forsterite content (Fo_{90}) are grayish white to light yellowish green and deeply yellowish green, respectively (Jan and Khan, 1996). XRD and EPMA data reveal that the acicular inclusions in the peridot are the magnesian iron borate mineral ludwigite, which has chemical formula $(Ti_{0.011}Cr_{0.041}Fe^{3+}_{0.947})_{1.0}(Mg_{1.085}Fe^{2+}_{0.897}Mn_{0.004}Ni_{0.013})_{2.00}B_{1.00}O_5$ (Jan and Khan, 1996).

1.2 Objectives

The purpose of the present research is:

- (1) To conduct mineralogical and geochemical studies of Sapat dunite and peridot in order to identify the processes involved in the formation of peridot in its host rock.
- (2) To study the origin of peridot and the host rock.

1.3 Location and accessibility of the area

The Sapat area is situated in the north of Naran ($34^{\circ}54'17''$ N and $73^{\circ}38'51''$ E) and Souch village ($34^{\circ}56'29''$ N and $73^{\circ}42'40''$ E; Fig.1.1). The access to Sapat is through Jal Kot Nala from Dassu, Kohistan and Sohch through Naran. A foot/mule track connects Sapat with both the localities. Naran, which is a hilly resort, lies at a distance of 115 km from Islamabad and takes approximately six to seven hours by road. Further, thirty hours of walk is required from Sohch village to reach the peridot mine area (Fig. 1.2).

1.4 Climate and habitation

The Sapat area is influenced by the pleasant summer of the Kaghan valley. In the month of May the temperature averages maximum 11°C to minimum of 3°C . In winter snow covers roads beyond Naran. Most of the population in the Kaghan-Naran region is nomadic.

1.5 Relief and topography

The Kaghan valley and its surroundings are known for lush green forests, meadows and landscapes. Mountains range from 3600 to 5000 m and more high above sea level. The eastern side of the Kaghan valley makes high ridges as compared to its western side (Fig 1.3).

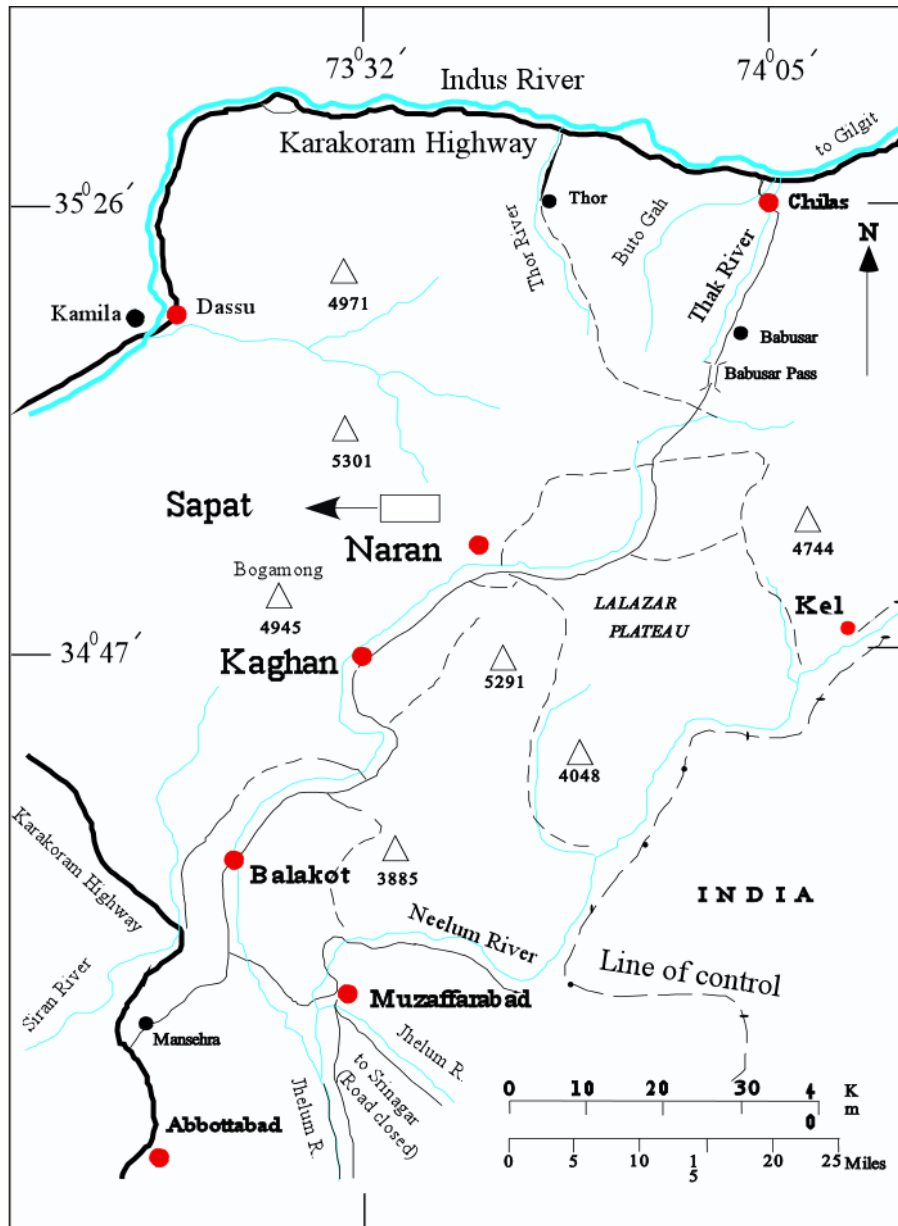


Figure 1.1. Location map of Sapat area, Naran-Kohistan (after Khan and Kausar, 2010).



Figure 1.2. A generalized view of the peridot mining area looking northward from the Sohch village.



Figure 1.3. High peaked mountains surrounding the Kaghan valley.

1.6 Previous work

Ultramafic and mafic rocks occur in the thesis area. Jan et al. (1993) named it Sapat complex, which occupies the base of the Kohistan island arc as cumulates. Jan and Khan (1996) reported ludwigite inclusions in a peridot crystal and Khan and Kausar (1996) reported magnetite as the pathfinder mineral for the peridot. Khan et al. (2004) correlated the complex with the Jijal complex. Hussain (2005) opined hydrothermal origin for the peridot whereas Khan et al. (2000) had described it as upper part of the mantle material. Bouilhol et al. (2012) described the origin of peridot mineralization due to subduction-derived fluids.

1.7 Methodology

Representative rock and peridot samples were collected from the Sapat area for petrographic, mineral chemistry and whole rock geochemical studies. X-Ray Diffractometer (XRD) was used to identify mineral composition of the peridot-host rock. Electron Probe Microanalyzer (EPMA) study was conducted for mineral analysis. Inductively coupled plasma mass spectrometry (ICP-MS) was used for the whole rock chemical analysis.

CHAPTER 2

GEOLOGY, TECTONIC SETTING AND GEOCHEMISTRY

2.1 Introduction

The Kohistan island arc (KIA) occupies an area between Karakoram and the Indian plates (e.g. Tahirkheli et al., 1979; Honneger et al., 1982) (Fig. 2.1) and formed possibly in Mesozoic times (Bard et al., 1980; Bard 1983; Coward et al., 1986) by the northward subduction of the Neo-tethyan oceanic plate. It welded in the north with the Karakoram plate. Here the contact is known as the Main Karakoram Thrust (MKT). The KIA overrides the higher Himalayas of the Indian plate. The contact is marked by a thrust fault known as the Main Mantle Thrust (MMT) (e.g. Tahirkheli et al., 1979; Coward et al., 1987). Ophiolitic mélanges occupy the MKT and MMT (Tahirkheli 1982; Kazmi et al., 1984). The MMT passes through the Sapat area near the watersheds between the Kohistan and Hazara districts

As already stated, the entire area of North Pakistan has been investigated geologically (e.g. Bender and Raza, 1995; Kazmi and Jan, 1997). There are four tectonic units, exposed in North Pakistan. From north to south (1) the Kohistan island arc (e.g. Tahirkheli et al., 1979; Bard 1983), (2) the MMT, comprising imbricate metasedimentary, metavolcanic and ophiolitic rocks (e.g. Shams et al., 1980; Kazmi et al., 1984), (3) the back-arc basin assemblages, named as the Jaglot group (Gilgit formation, Gashu-confluence volcanics, Thelichi formation; Khan, 1994) and (4) the Indian plate comprising orthogneiss, schists and marbles (Ghazanfar et al., 1991; Khan et al., 1995; Anczkiewicz et al., 2001) (Figs. 2.1, 2.2).

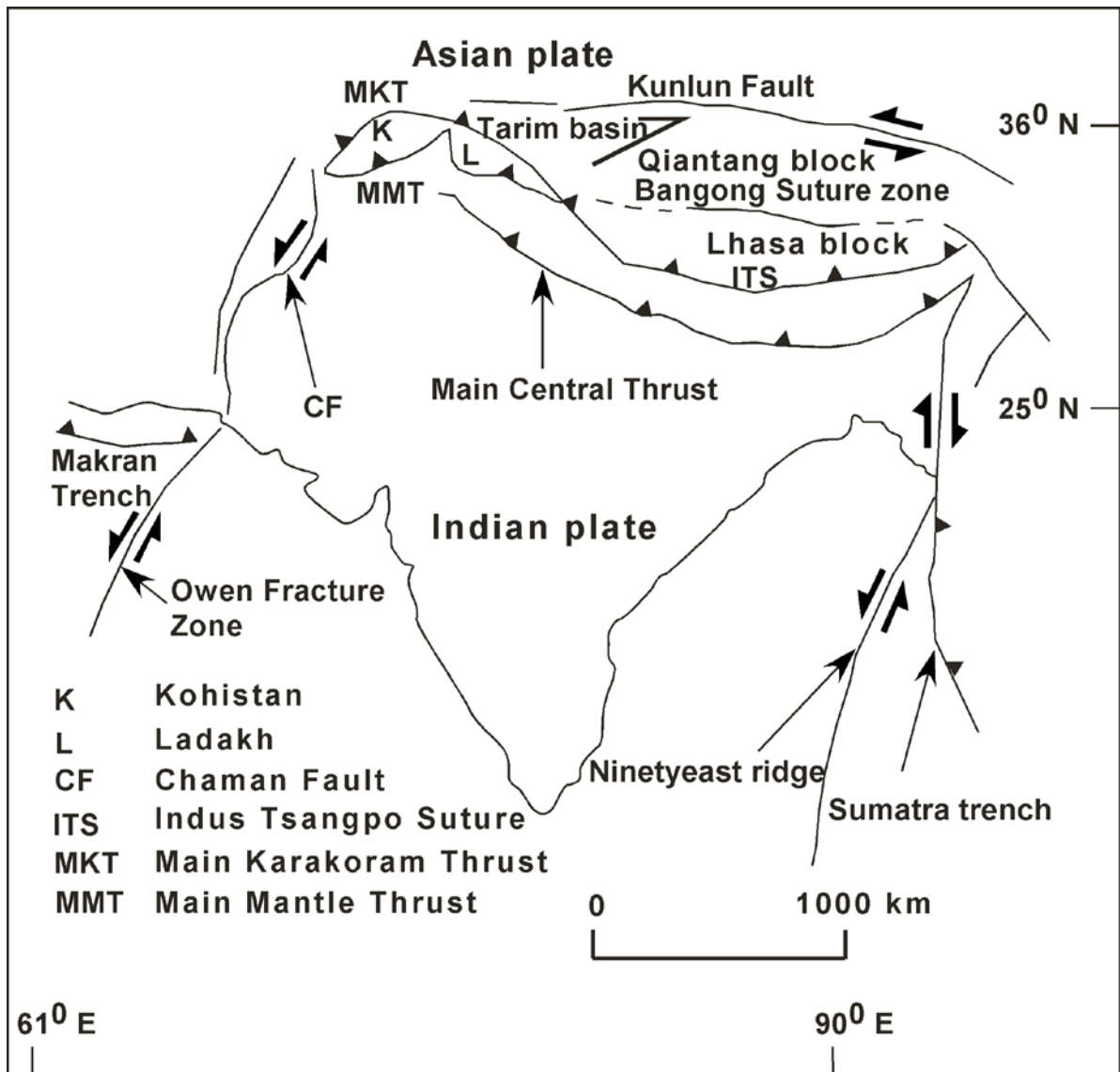


Figure 2.1. Regional tectonic map showing Kohistan-Ladakh island arc, Asian and Indian plates (after Khan et al., 2011).

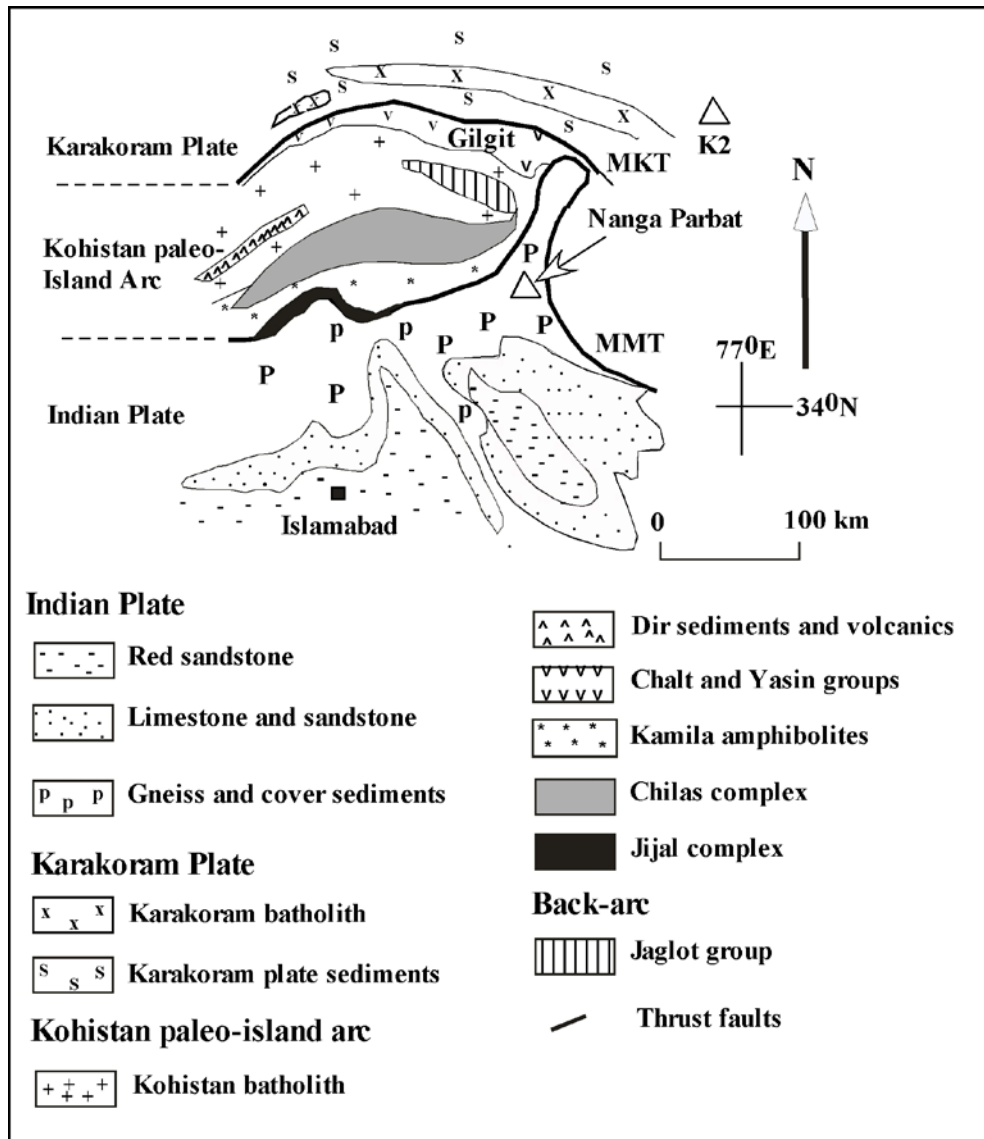


Figure 2.2. Regional geological and tectonic set up of the paleo-Kohistan island arc-back arc (after Khan et al., 2011).

The Kohistan island arc (KIA) covers a surface area of ~36,000 km² in North Pakistan. The predominant rock type in KIA is amphibolites, igneous, sedimentary and other metamorphic rocks that makeup the composition of the entire arc crust. Many researchers including Jan (1977, 1979), Tahirkheli (1979), Chaudhry et al. (1974b,1984), Petterson and Windley (1985), Ghazanfar et al. (1991), Khan, T et al. (1994, 1996, 1997, 2007, 2011), Khan, M.A et al. (1989, 1993), Sullivan et al. (1993), Treloar et al. (1996), Ringuette et al. (1998), Yamamoto and Nakamura (2000), Schaltegger et al. (2002), Khan, S.D et al. (2009) and Rehman et al. (2011) tried to systematize and synthesize the general geology, petrology, geochemistry, stratigraphy and geochronology of the KIA.

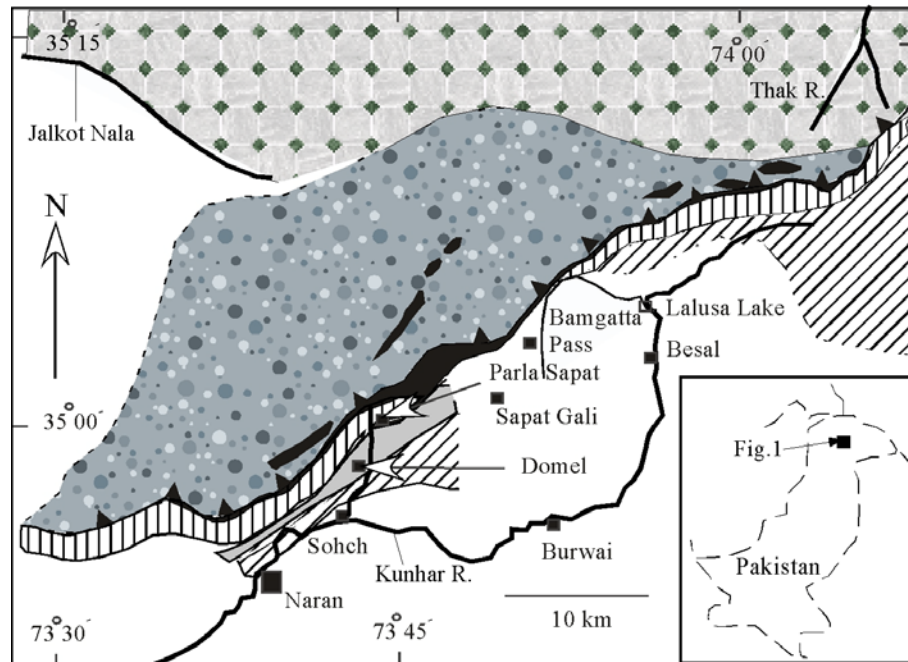
Treloar et al (1996) reappraised the geology of KIA and proposed that at about 100 Ma, it sutured first to the Asian plate (Karakoram microplate). Rehman et al. (2011) also described that the KIA collided with the Asian plate and later with the Indian plate forming Northern and Southern suture, respectively. Burg et al. (1998) presented new data, information and interpretation, various developmental stages and origin of KIA. According to Burg and his co-workers the KIA comprises structurally composite but more or less a coherent sequences of an intraoceanic island arc comprising 30-40 km thick section of metamorphosed plutonic, volcanic and sedimentary rocks. The entire island arc assemblage represents calc-alkaline plutons overlain by volcanic and low grade metasedimentary rocks. Immediate to the Indian plate in the hanging wall are the Jijal and the Sapat complexes. The Jijal complex is a tectonic wedge covering about 150 km² area to the north of MMT (e. g. Jan and Howie, 1981; Jan and Windley, 1990; Miller et al., 1991). The rocks include ultramafics and garnet granulites derived from feldspathic peridotites, pyroxenites, troctolites, olivine gabbros and gabbro-norites, and may represent cumulates in the deepest part of the arc. The Sapat complex also occurs just above the MMT and consists of ultramafics overlain by the mafics.

2.2 Local geology of the Sapat area




Khan et al. (1995) reported talc carbonate schist and greenschist metavolcanics intercalated with graphitic schists and phyllites of the Parla Sapat unit of the Indian plate near the contact with the Sapat complex (Fig. 2.3). They also reported marble bands together with calcareous schist from the same area. In Swat area, the Alpurai schist lying in the lower part of the MMT of the Indian plate depicts similar lithological characteristics (e.g. Kazmi et al., 1984).

The lens shaped Sapat complex named as Sapat peridotite (Bouilhol et al., 2009), which is 12km long and 1km wide contains composite mass of metaharzburgites, dunites, pyroxenites and metagabbros (Fig. 2.3). It has lower contact with the quartz-mica graphitic schist of the Indian continental plate, marked by a thrust fault. The fault planes dip northward with high angles about 60° to 70° and at places with opposite dips. However, the strike remains uniform N50° E at the average, and N30° E along the contact.


The magmatic stratigraphy of the Sapat complex has been worked out in the Ratti Gatti valley (e.g. Jan et al., 1993). The complex comprises isotropic and layered gabbros and layered to massive ultramafics with basal serpentinitic mylonites. The layered ultramafics include dunite-pyroxenite-gabbro-anorthosite layers, thinly layered dunite, pyroxenite, homogeneous dunite and serpentinitized dunite with thin chromite layers (e.g. Jan et al., 1993; Fig. 2.4).



Indian Plate Rocks

-  Parla Sapat Unit-mainly schists
-  Domel Unit- mainly calcareous
-  Granitic Gneisses

Kohistan Island Arc Rocks

-  Nat Metavolcanic Unit-mainly metabasalts

Sapat Complex






-  Gabbros
-  Cumulates and dunite
-  MMT
-  River/stream
-  Settlement

Figure 2.3. Geological map of the Sapat and the surrounding areas (reproduced from Khan et al., 1995).

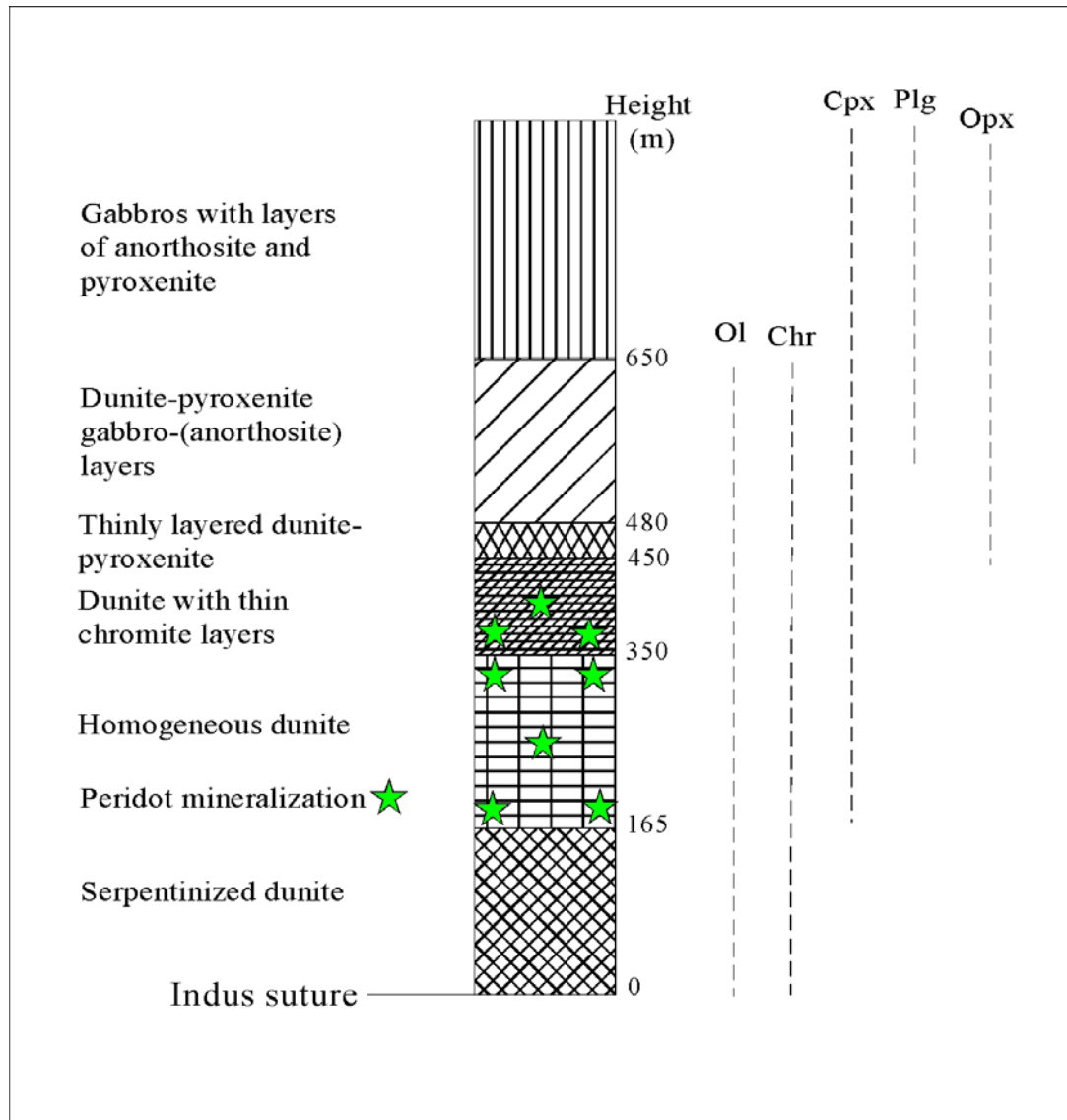


Figure 2.4. Cross section of the Sapat Complex showing peridot mineralization (reproduced after Jan et al., 1993). Symbols: Cpx= Clinopyroxene; Opx= Orthopyroxene; Plg= Plagioclase; Ol=Olivine; Chr= Chromite

The ultramafic basal part (focus of this research) is about half a kilometer thick and comprises dunite with minor streaks and layers of chromite (Fig. 2.5). It occurs to the southeast of West Sapat Gali, and to the north of Rah Wali Sapat (Parla Sapat, Kaghan-Naran area) and to the west of Ratti Gatti (Kohistan area). The massive dunite containing chromites is sheared and fractured. The fractures contain peridot (gem-olivine),

clinocrysotile, serpentine and magnetite (e.g. Kausar and Khan, 1996; Figs. 2.6, 2.7) and calcite-olivine bearing veins (Bouilhol et al., 2012).

Two-pyroxene gabbros, part of the Sapat mafic-ultramafic complex, are deformed and show medium to coarse-grained, hypidiomorphic and equigranular to subporphyritic textures. The gabbros mainly consist of plagioclase, clinopyroxene, amphibole, epidote and chlorite with titanite, magnetite, ilmenite \pm quartz. Clinopyroxene is rimmed by hornblende. Plagioclase shows alteration to epidote and chlorite. Ilmenite is surrounded by titanite and at places occurs in the form of tiny relics.

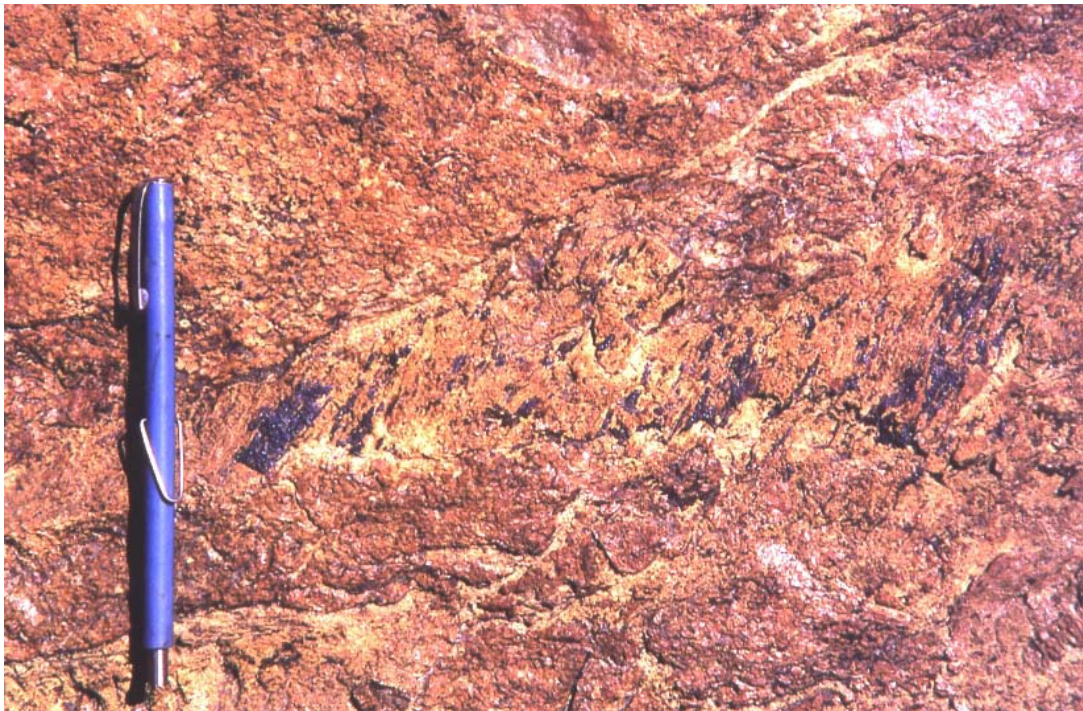


Figure 2.5. Sheared dunite containing chromite showing orientation along the shearing planes.

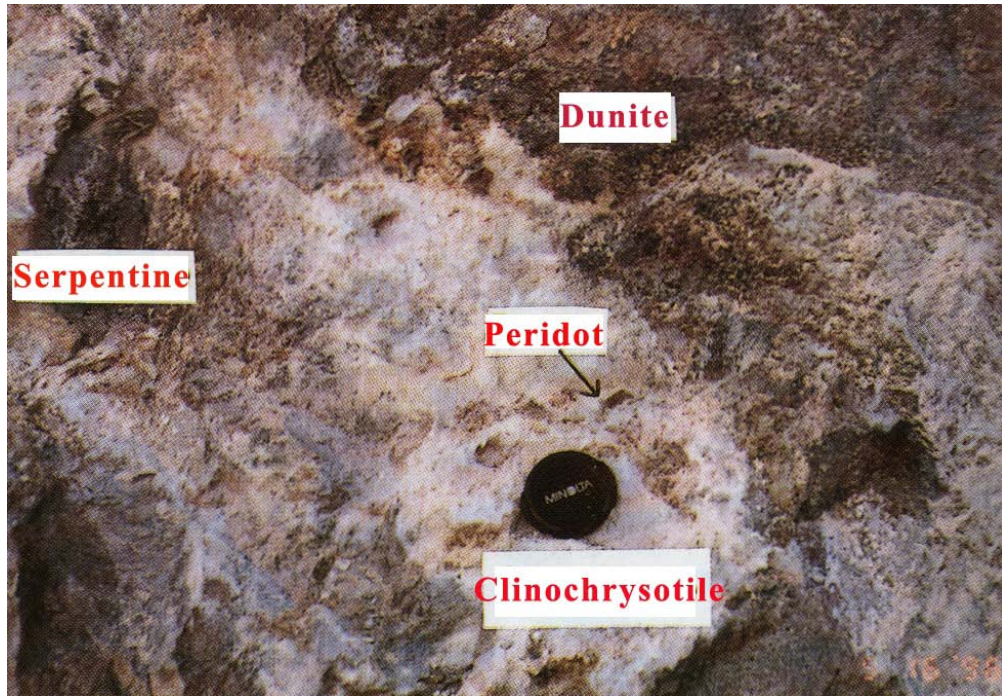


Figure 2.6. Fracture-filled peridot, clinocrysotile and antigorite in sheared dunite of the area (after Kausar and Khan, 1996).



Figure 2.7. Photograph showing magnetite grains (black) embedded in clinocrysotile (milky white).

2.3. Petrography of the peridot-bearing dunite

Olivine, titanite, antigorite, clinocrysotile and magnetite are the minerals constituting the rock (Fig. 2.8). Rutile is found as an accessory mineral. Olivine is present in the ground mass whereas peridots occupy the sheared parts. Peridots are zoned by antigorite and seem to replace them. At places, peridot relics are seen within the antigorite. Peridot contains two phase (water liquid and vapour) fluid inclusions may be primary and/or secondary ranging in size up to about 4 μm . Secondary inclusions cross cut the primary ones. Olivine and peridot phenocrysts depict ribbon structure. Magnetite grains are seen to develop across the peridot grain.

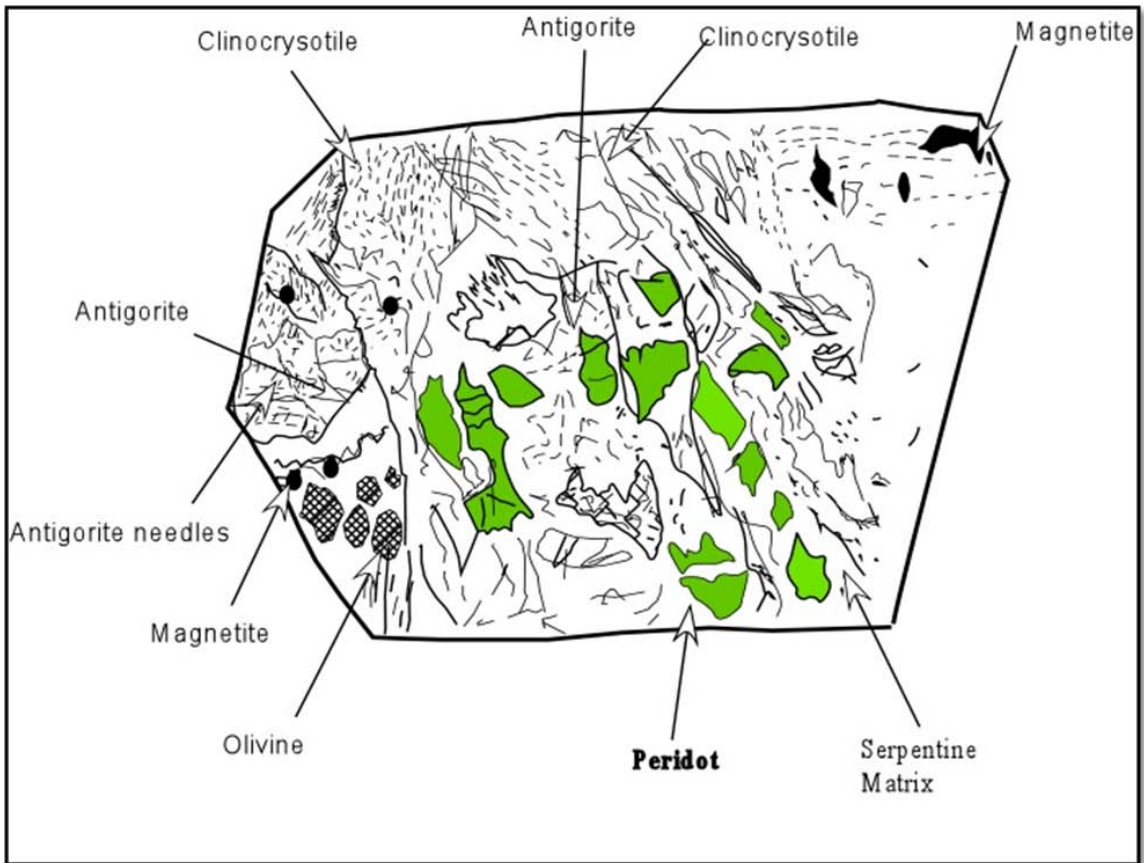


Figure 2.8. Sketch showing minerals and texture of sheared dunite containing peridot of the Sapat mafic-ultramafic complex.

2.4 XRD analysis

X-ray diffraction analysis was made on Rigaku-Geiger Flex X-Ray Diffractometer to identify peridot clinochrysotile and magnetite in the host sheared dunite (Fig. 2.9).

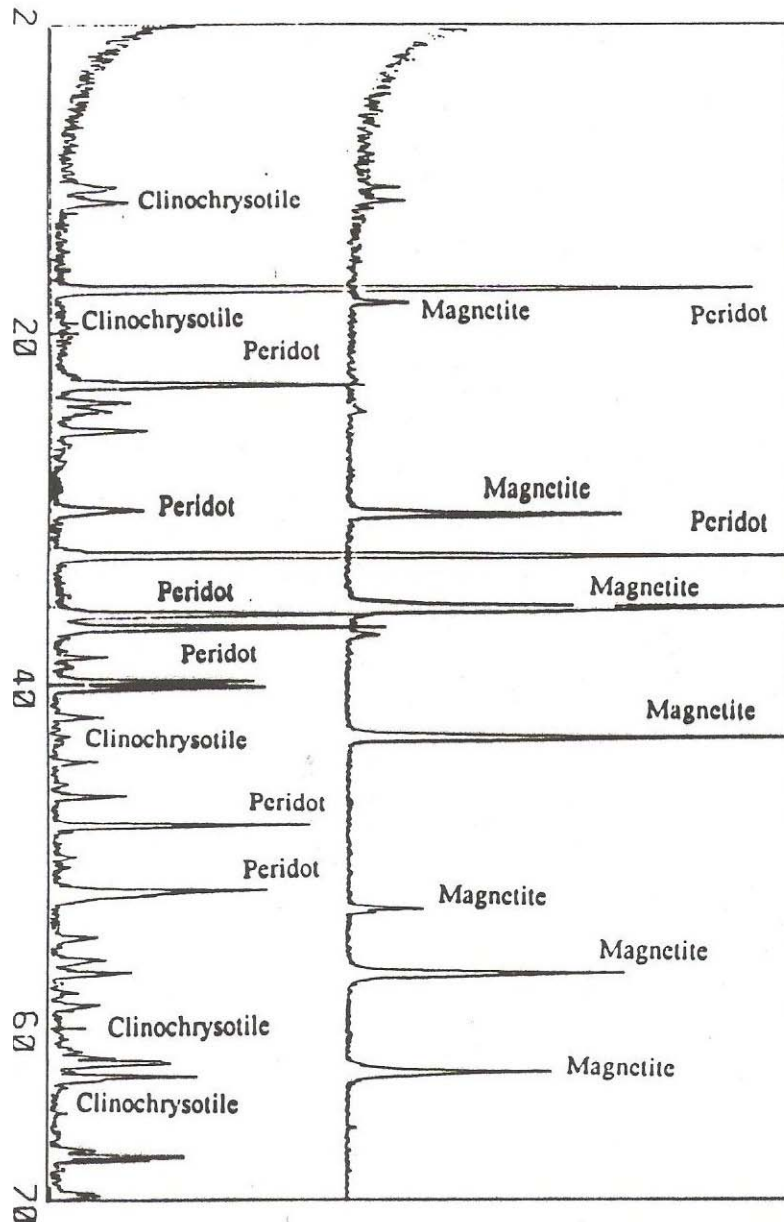


Figure 2.9. X-ray diffraction (XRD) analysis patterns of rock-powdered sample from Sapat area showing peridot, clinochrysotile and magnetite (after Kausar and Khan, 1996).

2.5 Mineral chemistry

Mineralogical studies on limited number of peridot samples were conducted using Electron Probe Micro-Analyzer (EPMA) and X-ray Diffraction (XRD). Olivine, chromite and chromian spinel chemical compositions were also determined by EPMA. EPMA analyses were conducted with 15kV voltage and 12nA beam current 1- μ m diameter. The correction procedure was based on ZAF method. Fe^{2+} and Fe^{3+} content of chromite and chromian spinel is calculated assuming spinel stoichiometry.

2.5.1 EPMA analysis

Peridot grains were analyzed for silicon, titanium, aluminum, chromium, iron, manganese, nickel, magnesium, calcium, sodium and potassium. The Asitmex and Taylor standard samples of the same element oxides were used. Thirty nine points were analyzed, out of which thirty six were of peridot and three were of serpentine compositions (Table 2.1). Back-scattered image of the peridot grain showing analyzed spots (Fig. 2.10) and the relative abundances of Mg, Fe and Ca + Mn in peridot are shown in figure 2.11. Element mapping for $\text{MgK}\alpha$, $\text{FeK}\alpha$ (Figs. 2.12 and 2.13) and $\text{MnK}\alpha$ at 15 Kv, accelerating current; 100nA, sample current and 0.03 seconds, sampling time, is obtained by stage scan method in which the beam, 1- μ m diameter, was kept fixed on a moving stage. During scanning, step size 0.029 mm in the X and Y directions each was maintained. The total area thus scanned is 14. 848 x 14. 848. Compositional mapping shows fresh and the deformed parts indicating high Mg content at the average of Fo_{91} and at a few points, Fo_{92} and rarely Fo_{95} , and comparatively lower Mg and higher Fe contents in the deformed part as compared to the fresh part (Fig. 2.13).

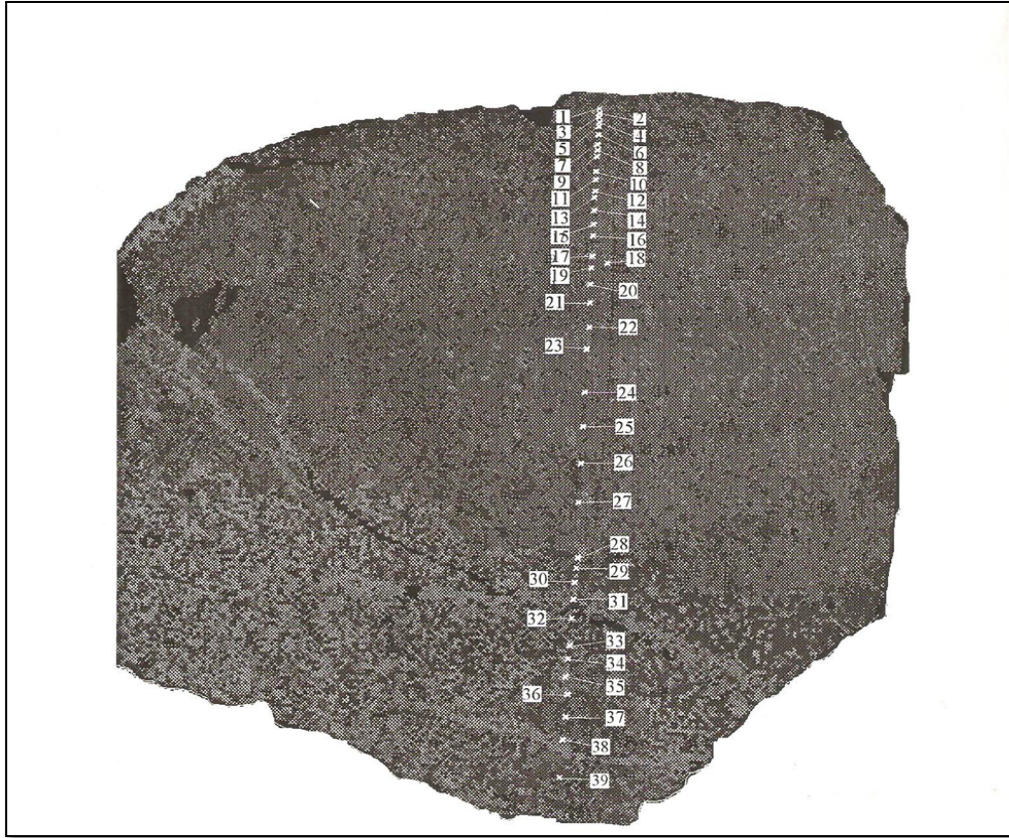


Figure 2.10. Back scattered image of the peridot grain showing the analyzed spots.

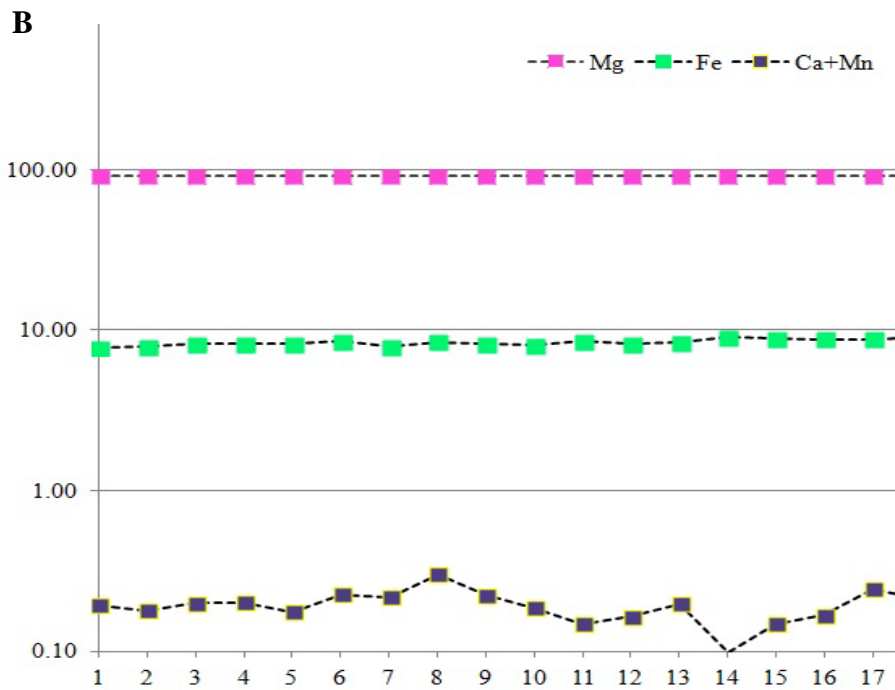
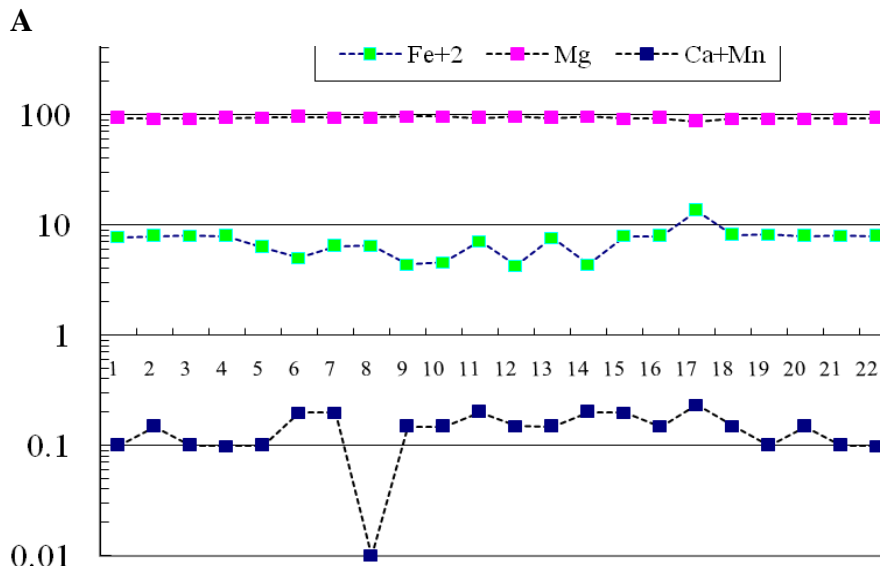


Figure 2.11. EPMA data of a peridot grain showing relative abundances of Mg, Fe and Ca+Mn ; A represents 22 analyzed points; B represents 23-39 analyzed spots.

Table 2.1. Electron microprobe data of peridot and serpentine from the Sapat area.

Sample points	1	2	3	4	5	6	7	8	9	10	11	12	13	14	15	16	17	18	19	20
SiO ₂	42.71	42.55	41.86	42.90	42.09	42.39	42.54	42.40	40.74	42.23	40.64	40.51	38.63	40.24	42.16	40.36	41.66	42.53	38.84	43.01
TiO ₂		0.02	0.01	0.01		0.01		0.00		0.00	0.00	0.00	0.01			0.01		0.00	0.01	0.01
Al ₂ O ₃		0.01	0.03		0.01				0.01		0.00	0.01		0.01	0.02		0.02			0.00
FeO	7.82	7.75	8.04	8.18	8.36	7.97	7.93	9.39	8.22	8.18	8.62	8.20	8.45	9.08	8.84	8.85	8.36	8.62	8.61	8.29
Cr ₂ O ₃							0.02						0.02	0.01	0.04	0.01	0.03		0.02	
MnO	0.19	0.18	0.19	0.20	0.17	0.03	0.21	0.29	0.22	0.18	0.15	0.16	0.20	0.10	0.15	0.17	0.23	0.20	0.32	0.21
NiO	0.29	0.36	0.34	0.23	0.31	0.23	0.04	0.33	0.33	0.41	0.48	0.29	0.42	0.37	0.27	0.23	0.28	0.31	0.33	0.22
MgO	51.78	50.85	50.17	50.95	51.94	47.51	51.71	50.97	51.24	51.87	51.77	51.04	51.57	51.50	51.03	51.33	48.57	48.17	51.28	49.44
CaO	0.03	0.01	0.01	0.02	0.01	0.01	0.02	0.01		0.02	0.00	0.02		0.01	0.02	0.01	0.01	0.00	0.01	0.00
Total	102.82	101.71	100.65	102.49	102.90	98.31	102.74	102.39	100.77	102.89	101.67	100.32	99.30	101.32	102.52	100.97	99.17	99.84	99.43	101.18
Cations on the basis of 4 oxygen																				
Si	1.0075	1.0139	1.0101	1.0155	0.9959	1.0424	1.0052	1.0076	0.9865	0.9986	0.9782	0.987	0.9552	0.974	1.0025	0.9784	1.021	1.0342	0.9595	1.03
Ti		0.017	0.0003	0.0003		0.0002							0.0001	0		0.0002			0.0002	0.0001
Al		0.0003	0.0008		0.0003				0.0002		0.0001	0.0004		0.0004	0.0005		0.0006			
Fe	0.1542	0.1544	0.1622	0.1619	0.1655	0.1639	0.1567	0.1668	0.1665	0.1617	0.1736	0.1666	0.1748	0.1838	0.1757	0.1795	0.1713	0.1753	0.1779	0.1661
Cr							0.0004						0.0004	0.0002	0.0008	0.0001	0.0006		0.0004	
Mn	0.0038	0.0035	0.0039	0.0039	0.0035	0.0043	0.0043	0.0059	0.0045	0.0037	0.003	0.0033	0.0041	0.002	0.0029	0.0034	0.0047	0.0041	0.0068	0.0042
Ni	0.0056	0.0068	0.0067	0.0044	0.0059	0.0045	0.0058	0.0063	0.0065	0.0079	0.0093	0.0057	0.0083	0.0072	0.0051	0.0045	0.0056	0.0061	0.0065	0.0042
Mg	1.8207	1.8062	1.805	1.7977	1.8325	1.7419	1.8217	1.8057	1.8491	1.8289	1.8575	1.8493	1.9014	1.858	1.8088	1.8551	1.7745	1.746	1.8885	1.765
Ca	0.0008	0.0002	0.0004	0.0005	0.0003	0.0002	0.0005	0.0002		0.0006		0.0005		0.0002	0.0005	0.0001	0.003	0.0001	0.0003	0.0001
Cation percentages																				
Fe	7.79	7.86	8.23	8.24	8.27	8.58	7.90	8.43	8.24	8.11	8.53	8.25	8.40	8.99	8.84	8.81	8.77	9.10	8.58	8.58
Mg	91.98	91.95	91.55	91.53	91.54	91.18	91.86	91.26	91.54	91.68	91.32	91.56	91.40	90.90	90.99	91.02	90.84	90.68	91.08	91.20
Ca+Mn	0.19	0.18	0.20	0.20	0.18	0.23	0.22	0.30	0.22	0.19	0.15	0.16	0.20	0.10	0.15	0.17	0.24	0.21	0.33	0.22
Fe/Fe+Mg	0.08	0.08	0.08	0.08	0.08	0.09	0.08	0.08	0.08	0.08	0.09	0.08	0.08	0.09	0.09	0.09	0.09	0.09	0.09	0.09
Mg/Fe+Mg	0.92	0.92	0.92	0.92	0.92	0.91	0.92	0.91	0.92	0.92	0.91	0.92	0.91	0.91	0.91	0.91	0.91	0.91	0.91	0.91

Table 1 continued.

	21	22	23	24	25	26	27	28	29	30	31	32	33	34	35	36	37	38	39
SiO ₂	43.65	43.67	42.81	41.33	44.40	43.03	42.67	40.48	19.31	41.83	39.54	37.51	42.11	38.25	39.35	35.24	40.63	40.34	37.64
TiO ₂		0.01	0.01			0.03		0.02	0.00		0.03	0.01	0.00				0.01		
Al ₂ O ₃	0.01			0.02	0.01	0.01		0.03	0.01		0.02	0.03	0.02						
FeO	8.50	8.60	8.63	9.02	6.65	8.56	6.64	4.41	14.99	4.61	4.65	2.01	8.80	1.81	8.71	8.97	8.91	8.81	9.17
Cr ₂ O ₃	0.00	0.02	0.00	0.01		0.00		0.06							0.02				
MnO	0.24	0.21	0.20	0.14	0.19	0.19	0.22	0.21	0.80	0.16	0.20	0.03	0.16		0.13	0.24	0.24	0.17	0.11
NiO	0.36	0.28	0.27	0.38	0.36	0.35	0.21	0.22	0.41	0.39	0.23		0.35	0.03	0.26	0.30	0.33	0.23	0.29
MgO	49.20	48.95	48.81	49.47	51.20	48.83	50.05	52.57	36.20	52.29	53.29	41.66	50.85	42.12	49.63	51.26	50.45	50.66	50.49
CaO	0.02	0.00	0.02	0.02	0.01	0.01	0.01	0.02	0.23		0.01	0.02	0.02	0.02	0.02	0.01	0.01	0.01	0.01
Total	101.98	101.74	100.76	100.40	102.82	101.00	99.80	98.00	71.96	99.27	97.97	81.28	102.31	82.03	98.11	96.02	100.58	100.23	97.72
Cation on the basis 4 oxygen																			
Si	1.0375	1.0401	1.0313	1.0053	1.0377	1.0337	1.029	0.9902	0.726	1.0084	1.9712	1.08	1.0035	1.063	0.9817	0.9103	0.9884	0.9843	0.9495
Ti		0.0002	0.0001			0.0005		0.0004			0.0005	0.0001					0.0002		
Al	0.0003			0.0007	0.0003	0.0002		0.0008	0.0003		0.0004	0.0011	0.0004						
Fe	0.1689	0.1712	0.174	0.1835	0.1299	0.1719	0.1338	0.0901	0.4714	0.0929	0.0956	0.0485	0.1753	0.043	0.1817	0.1938	0.1813	0.1798	0.1936
Cr		0.0003	0.0001	0.0002				0.0011							0.0004				
Mn	0.0048	0.0042	0.0041	0.0028	0.0038	0.0039	0.0045	0.0004	0.0256	0.0033	0.0042	0.0008	0.0032		0.0027	0.0052	0.005	0.0036	0.0024
Ni	0.0069	0.0054	0.0052	0.0074	0.0067	0.0068	0.0041	0.0042	0.0125	0.0075	0.0046		0.0067	0.0008	0.0053	0.0062	0.0064	0.0045	0.0059
Mg	1.7434	1.738	1.7531	1.7938	1.7836	1.7486	1.7994	1.9168	2.0287	1.8794	1.9515	1.7881	1.8065	1.7831	1.8459	1.974	1.8297	1.8431	1.8989
Ca	0.0005		0.0006	0.0005	0.0003	0.0001	0.0003	0.0004	0.0094		0.0002	0.0006	0.0006	0.0007	0.0005	0.0002	0.0003	0.0002	0.0002
Cation percentages																			
Fe	8.81	8.95	9.01	9.26	6.77	8.93	6.90	4.49	18.59	4.70	4.66	2.64	8.83	2.35	8.95	8.92	8.99	8.87	9.24
Mg	90.92	90.83	90.75	90.57	93.01	90.86	92.85	95.47	80.02	95.13	95.13	97.29	90.98	97.61	90.90	90.83	90.75	90.94	90.64
Ca+Mn	0.25	0.22	0.21	0.14	0.20	0.20	0.23	0.02	1.02	0.17	0.20	0.04	0.16		0.13	0.24	0.25	0.18	0.11
Fe/Fe+Mg	0.09	0.09	0.09	0.09	0.07	0.09	0.07	0.04	0.19	0.05	0.05	0.03	0.09	0.02	0.09	0.09	0.09	0.09	0.09
Mg/Fe+Mg	0.91	0.91	0.91	0.91	0.93	0.91	0.93	0.95	0.80	0.95	0.95	0.97	0.91	0.98	0.91	0.91	0.91	0.91	0.91

Serpentine. FeO expressed as total iron.

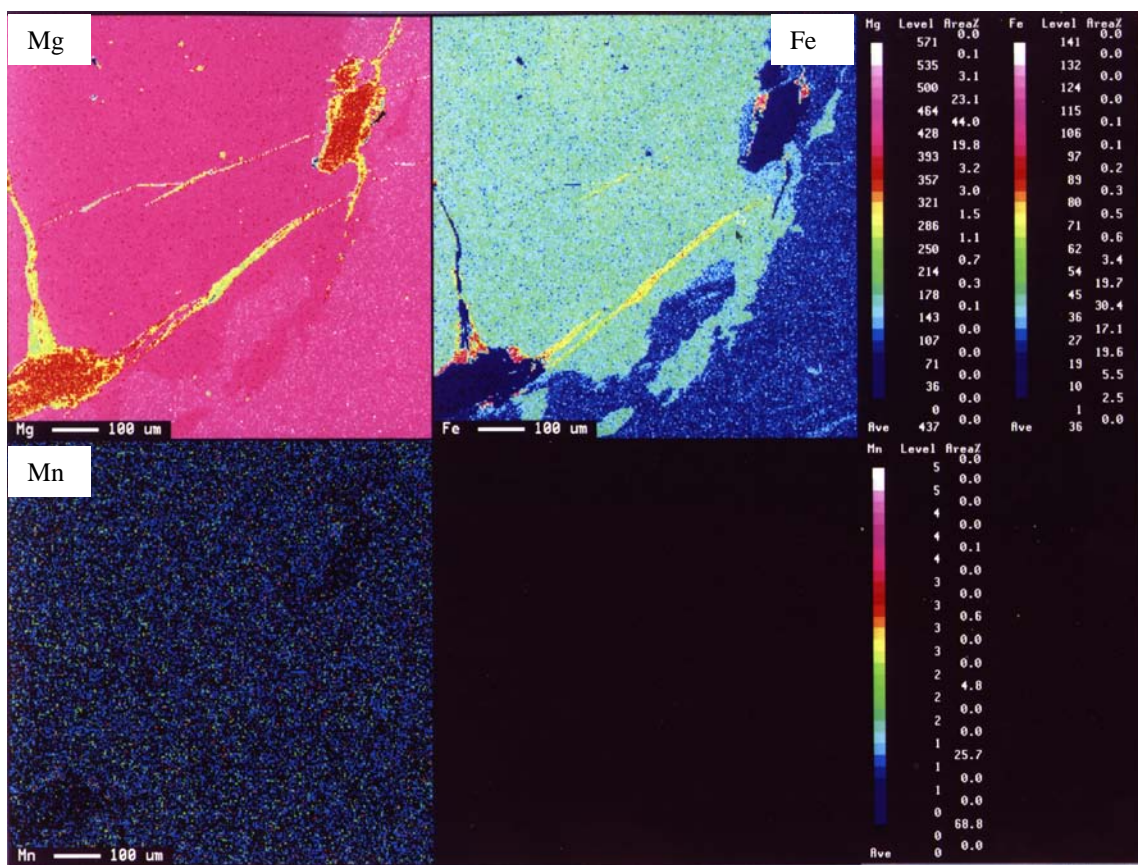


Figure 2.12. Compositional map showing the distribution of Mg and Fe relative to X-ray intensities of MgK α and Fe K α lines and the intensities range of each element are displayed as pseudocolors in the form of similar color pellet for each map.

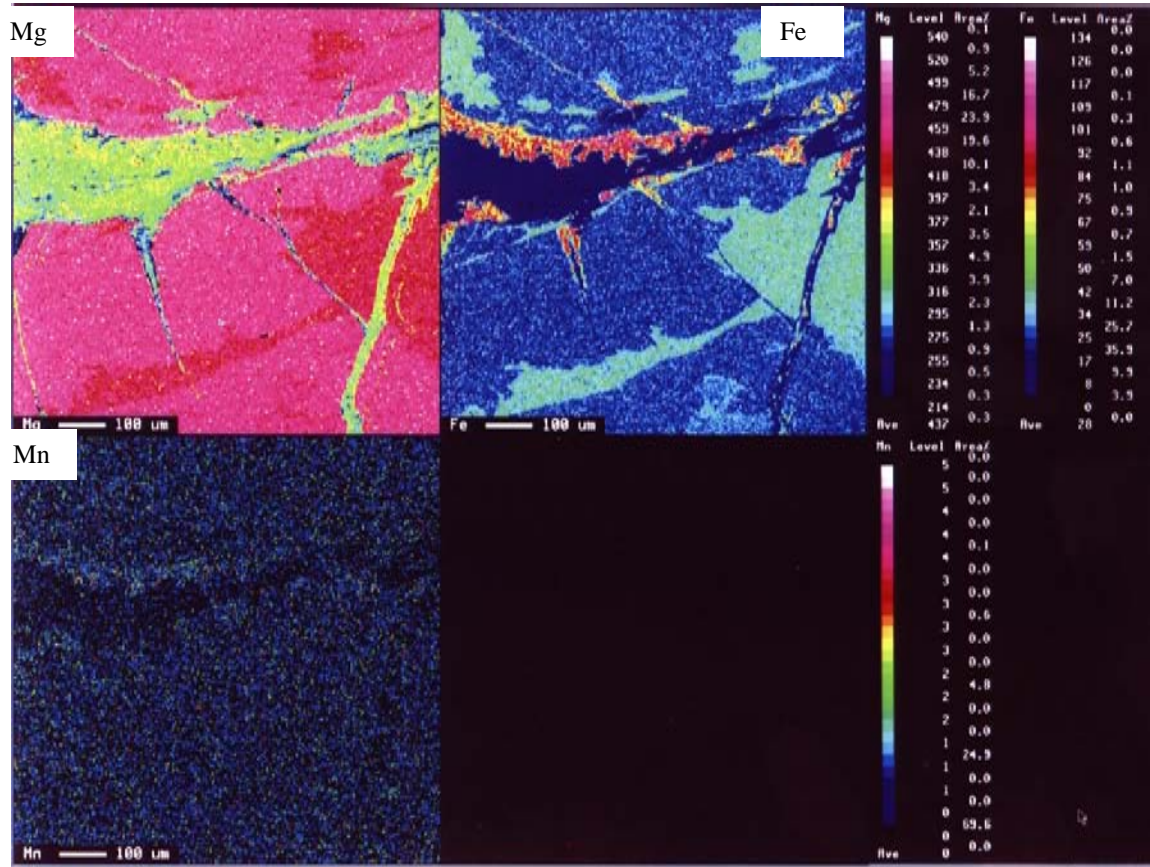


Figure 2.13. Compositional mapping of peridot grain showing Mg, Fe and Mn. Serpentine is developed in the microfractures of the deformed peridot grains. Mutual replacement of Mg and Fe is seen in the image.

2.6 EPMA analysis of olivine and chromian spinel from peridot-bearing dunite

Totally, 7 points of olivine and 12 points of chromian spinel were analyzed using EPMA (Fig. 2.14).

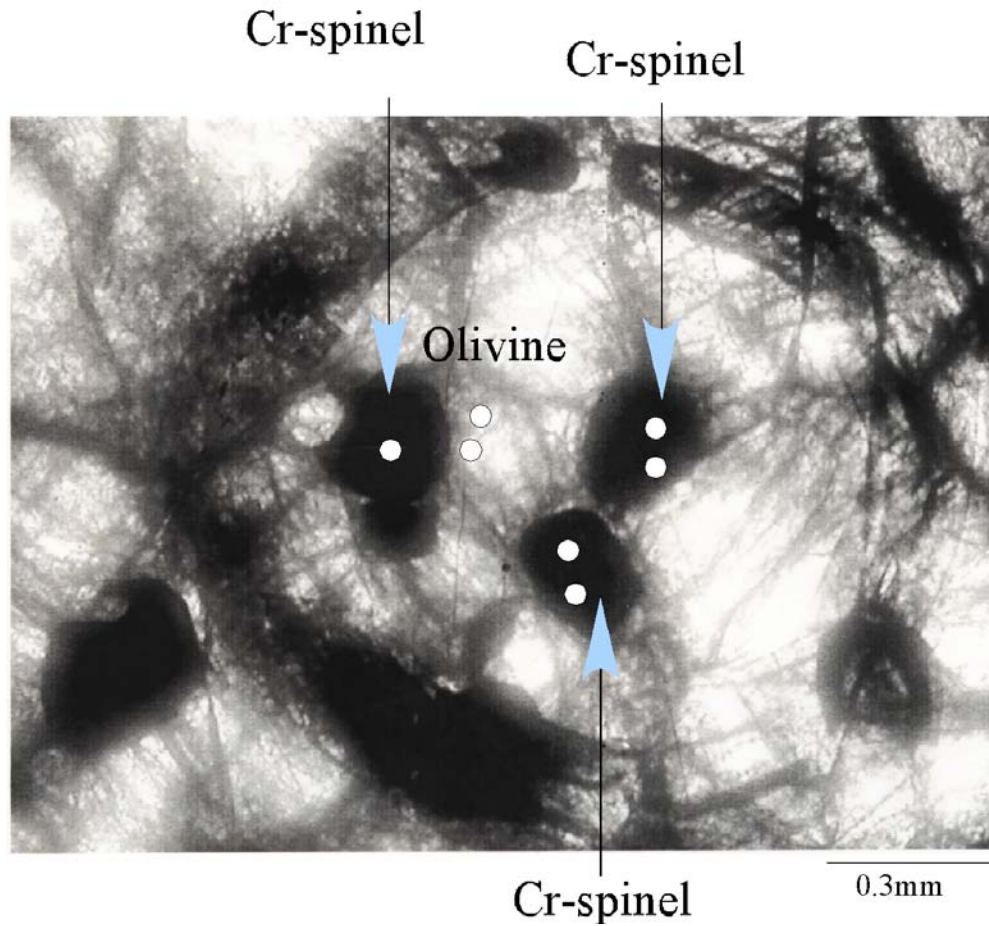


Figure 2.14. One of the back-scattered images of analyzed selected parts of olivine and chromian spinel (white spots) in the peridot-bearing dunite

2.6.1 Olivine analysis

The olivine analyses of the dunite are presented in table 2.2. In olivine MgO ranges from 52.84 to 51.61 wt% and the NiO, 0.45 to 0.30 wt%. The NiO shows slight variation with nearly constant forsterite content $(Mg) \times (100) / (Mg + Fe^{2+})$. Using the MgO-NiO diagram, the data fall in the mantle peridotites field (Fig. 2.15).

Table 2.2. Representative olivine data from dunite.

Sample points	1	2	3	4	5	6	7	8	9	10	11	12	13	14	15	16	17
SiO ₂	41.439	41.204	41.614	41.389	41.700	40.977	40.937	41.180	41.289	41.704	41.010	41.216	41.499	40.390	40.507	40.548	41.540
Al ₂ O ₃	0.019	0.011			0.008						0.002					0.002	
TiO ₂					0.001		0.053		0.016			0.009					
Cr ₂ O ₃	0.055	0.306		0.018	0.046	0.120	0.009		0.028	0.037		0.083				0.019	0.037
FeO	7.527	7.160	7.162	7.198	7.026	5.911	5.995	6.716	8.481	7.137	8.512	6.884	7.082	7.099	6.275	6.660	7.568
MnO	0.180	0.087	0.036	0.180	0.029	0.122	0.144	0.158	0.137	0.151	0.201	0.209	0.094	0.181	0.044	0.137	0.050
MgO	53.265	52.959	52.844	53.579	53.489	51.844	52.044	52.398	52.517	53.201	51.985	53.465	52.939	52.869	51.606	52.549	52.361
CaO		0.008	0.005	0.009		0.012		0.004			0.007		0.100	0.002	0.018	0.012	0.006
Na ₂ O	0.004	0.006		0.006	0.023			0.004	0.002	0.010		0.002	0.006	0.002		0.012	0.008
K ₂ O	0.006				0.014	0.015					0.009	0.001	0.001	0.005	0.011	0.012	0.004
NiO	0.421	0.347	0.425	0.259	0.359	0.296	0.358	0.450	0.348	0.209	0.332	0.083	0.415	0.354	0.348	0.387	0.371
Total	102.92	102.10	102.09	102.64	102.69	99.30	99.49	100.97	102.80	102.47	102.06	102.13	102.06	100.90	98.81	100.34	101.95
Cation based on 24 oxygens																	
Si	5.879	5.882	5.932	5.875	5.907	5.972	5.958	5.930	5.885	5.921	5.891	5.874	5.919	5.841	5.945	5.881	5.939
Ti		0.001						0.006		0.002		0.009					
Al	0.003	0.002			0.001						0.004					0.000	
Fe ²⁺	0.893	0.855	0.854	0.855	0.832	0.720	0.730	0.809	1.011	0.847	1.023	0.821	0.845	0.859	0.770	0.808	0.905
Mn	0.022	0.011	0.004	0.022	0.004	0.015	0.018	0.019	0.017	0.018	0.024	0.025	0.011	0.222	0.005	0.017	0.006
Mg	11.264	11.271	11.229	11.338	11.295	11.263	11.292	11.248	11.158	11.259	11.131	11.360	11.255	11.396	11.290	11.361	11.160
Ca		0.001	0.001	0.001		0.002		0.001	0.000		0.001		0.002	0.000	0.003	0.002	0.001
Na	0.001	0.002		0.002	0.006			0.001	0.001	0.003		0.006	0.002	0.001		0.004	0.002
K	0.001				0.003	0.003					0.002	0.001	0.000	0.001	0.002	0.002	0.001
Cr	0.006	0.035		0.002	0.005	0.014	0.001		0.003	41.000		0.009				0.002	0.004
Ni	0.048	0.040		0.030	0.041	0.035	0.042	0.052	0.040	0.024	0.038	0.312	0.048	0.041	0.041	0.448	0.043
Total	18.118	18.099	18.068	18.124	18.091	18.023	18.041	18.065	18.114	18.077	18.110	18.121	18.081	18.160	18.056	18.121	18.060
Mg#	92.655	92.950	92.934	92.991	93.136	93.988	93.929	93.292	91.693	93.001	91.587	93.263	93.019	92.995	93.614	93.362	92.499

Key: Mg# = $(Mg) \times (100) / (Mg + Fe^{2+})$; FeO expressed as total iron.

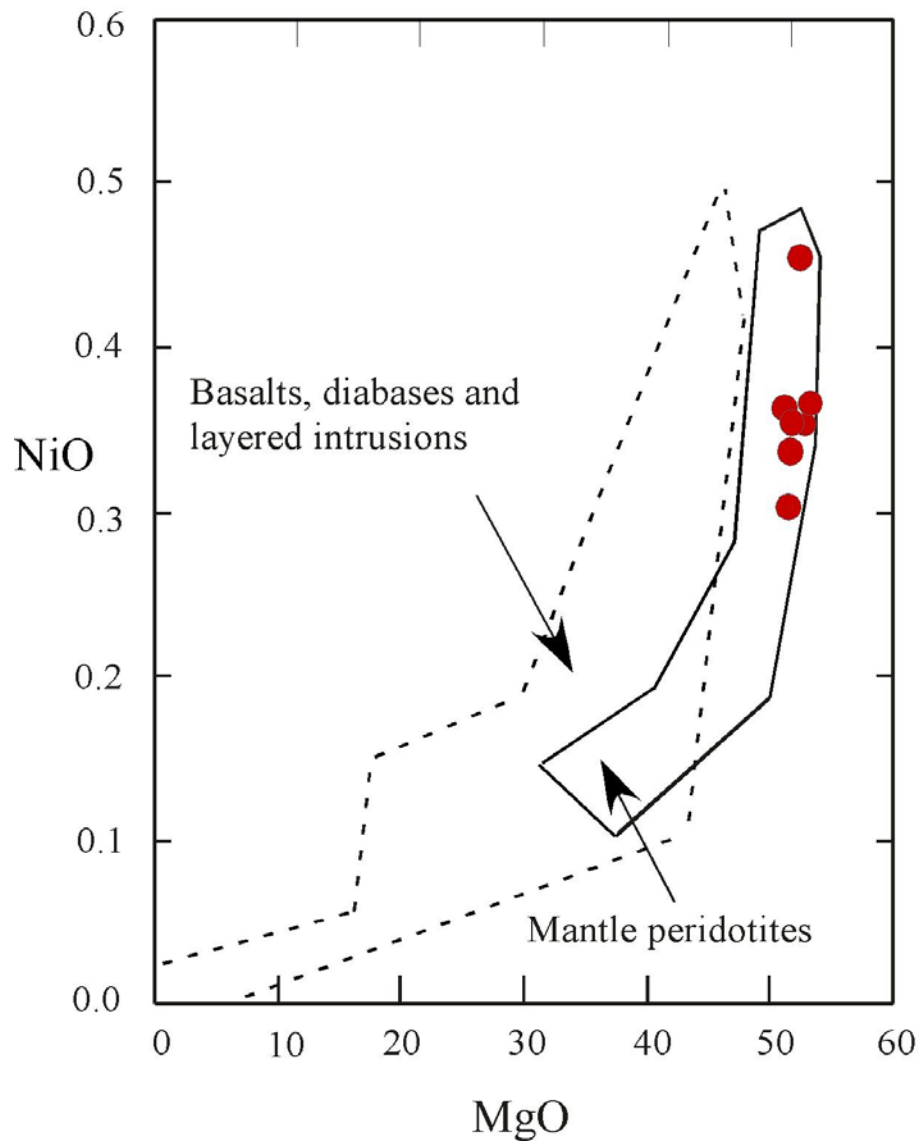


Figure 2.15. Variation diagram of MgO and NiO in olivine. Continuous lines: olivine from upper mantle peridotites; Broken lines: olivine of basalts, diabases and layered intrusions (after Fleet et al., 1977).

2.6.2 Chromian spinel analysis

The chromian spinel (Cr-spinel) shows Al₂O₃ ranging from 7.90 to 14.83 wt% and Cr₂O₃ from 50.66 to 54.42 wt % (Table 2.3). The Cr-spinel, which will be used for the interpretation of origin of dunite because of its primary nature, contains small amounts of TiO₂ (0.18-0.27 wt %) and shows relatively low Mg/(Mg+ Fe²⁺) (0.31-0.44) and high Cr/(Cr+Al) (0.70-0.82) ratios.

Table 2.3. Representative chromian spinel data of dunite from the Sapat complex.

Sample points	1	2	3	4	5	6	7	8	9	10	11	12
Al ₂ O ₃	14.29	14.49	14.22	14.21	14.28	13.67	12.63	12.82	14.83	7.90	14.32	11.95
TiO ₂	0.22	0.21	0.23	0.27	0.24	0.22	0.18	0.18	0.20	0.21	0.22	0.18
Cr ₂ O ₃	52.42	52.65	51.62	53.99	53.11	52.03	52.58	51.70	52.83	51.94	53.27	50.66
FeO	25.46	23.91	24.60	24.44	23.22	24.42	26.14	23.95	23.50	32.41	23.48	24.29
MnO	0.52	0.48	0.36	0.46	0.36	0.43	0.51	0.51	0.36	0.61	0.35	0.48
MgO	7.79	8.78	8.37	8.53	8.80	8.23	7.88	8.46	9.14	5.91	9.03	7.62
NiO		0.12			0.07		0.11	0.08	0.06	0.01	0.01	0.01
Total	100.70	100.52	99.40	101.90	100.08	99.00	100.03	97.70	100.84	98.99	100.68	95.19
Cation on the basis of 4 oxygen												
Al	0.550	0.554	0.552	0.539	0.549	0.534	0.492	0.508	0.564	0.321	0.547	0.489
Ti	0.005	0.005	0.006	0.006	0.006	0.005				0.005	0.005	
Cr	1.354	1.351	1.344	1.373	1.370	1.363	1.374	1.373	1.347	1.416	1.365	1.390
Fe ²⁺	0.611	0.564	0.585	0.584	0.566	0.586	0.599	0.564	0.554	0.683	0.560	0.595
Mn	0.014	0.013	0.010	0.013	0.010	0.012	0.014	0.014	0.010	0.018	0.010	0.014
Mg	0.379	0.425	0.411	0.409	0.428	0.406	0.388	0.423	0.439	0.303	0.436	0.394
Fe ³⁺	0.084	0.085	0.093	0.073	0.068	0.091	0.124	0.109	0.079	0.251	0.077	0.110
Total	3.00	3.00	3.00	3.00	3.00	3.00	2.99	2.99	2.99	3.00	3.00	2.99
Mg#	0.38	0.43	0.41	0.41	0.43	0.41	0.39	0.43	0.44	0.31	0.44	0.40
Cr#	0.71	0.71	0.71	0.72	0.71	0.72	0.74	0.73	0.70	0.82	0.71	0.74

Mg#, Mg/ (Mg+Fe²⁺); Cr#, Cr/(Cr+Al); FeO expressed as total iron.

Using Cr₂O₃ versus Al₂O₃ diagram of Franz and Wirth (2000) and Mg# (olivine) versus Cr# (spinel) of Pearce et al. (2000), the data plot in the olivine-spinel mantle array (OSMA) field of Arai (1994) (Figs.2.16 and 2.17). The Cr# and TiO₂ of Cr-spinel in the dunite of the Sapat complex characterize the dunite in the overlapping field of island arc and boninites (Fig. 2.18).

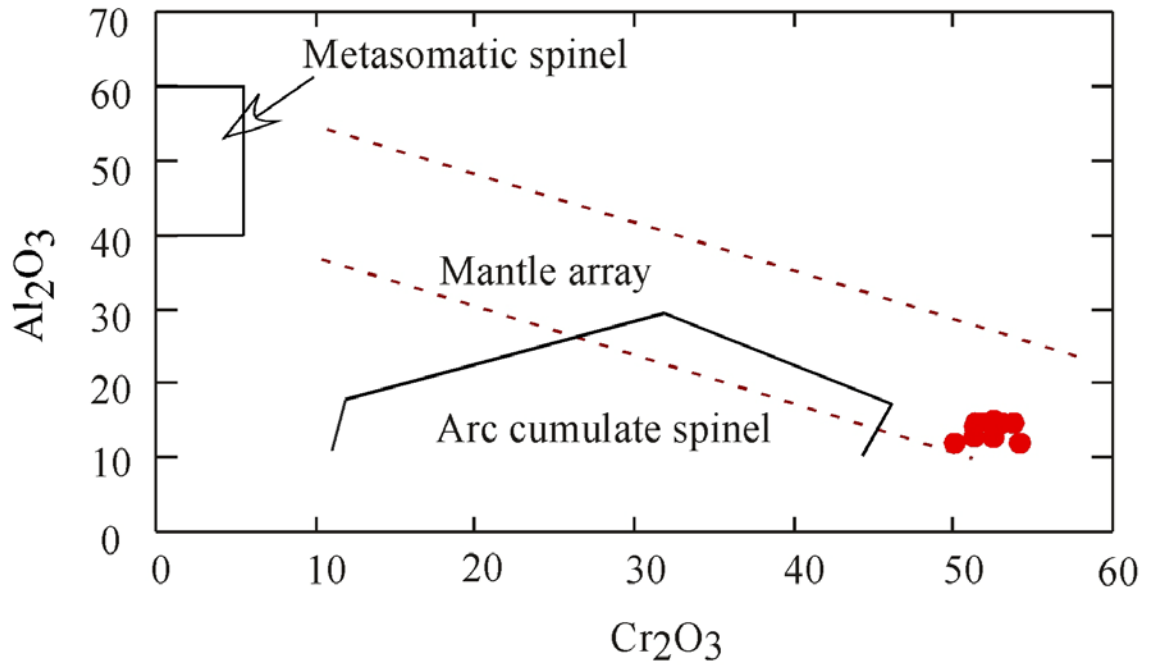


Figure 2.16. Al_2O_3 - Cr_2O_3 diagram showing chromian spinel of the dunite to occupy olivine-spinel mantle array field (after Franz and Wirth, 2000; Khan et al., 2004).

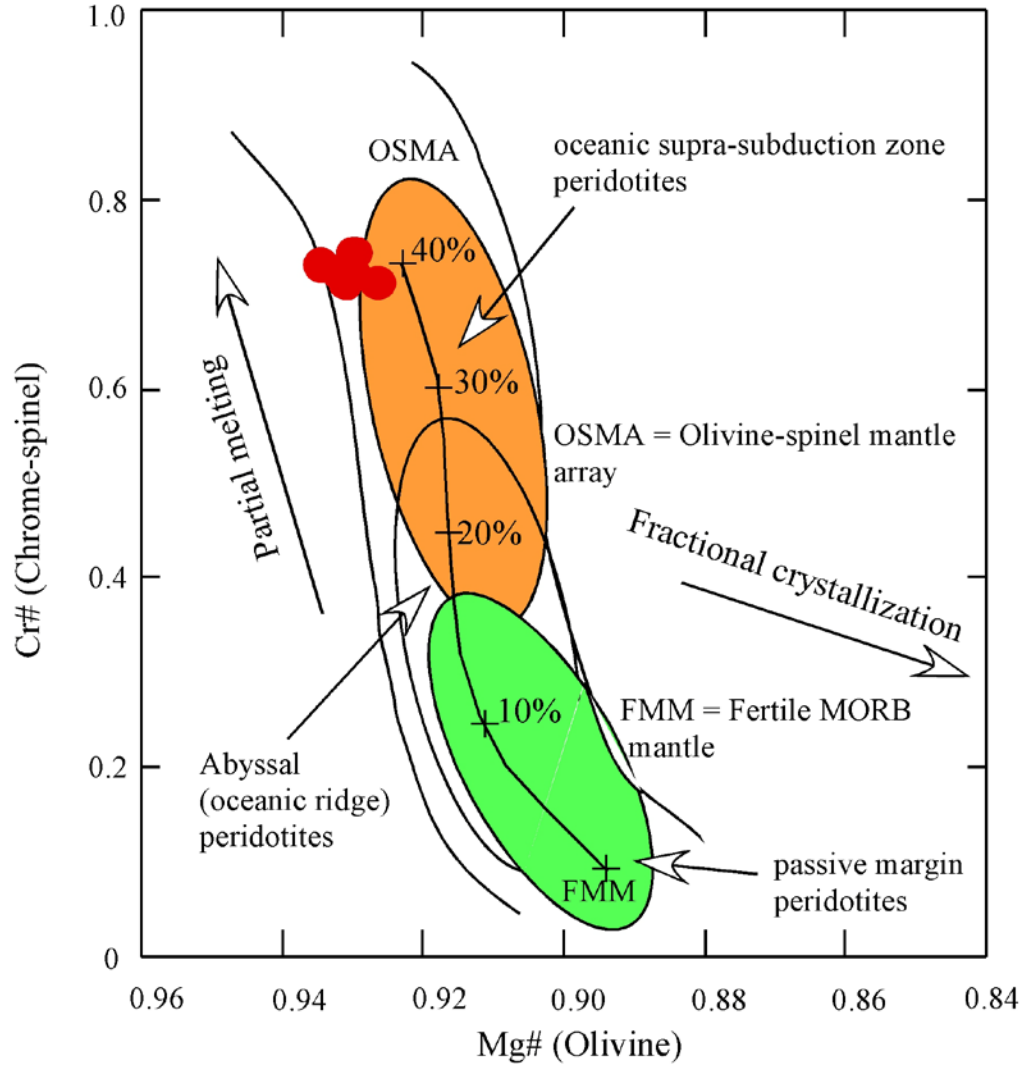


Figure 2.17. Cr# of chromian spinel versus Mg# of olivine in the dunite of the Sapat complex (reproduced from Pearce et al., 2000; Dick and Bullen, 1984; Arai, 1994).

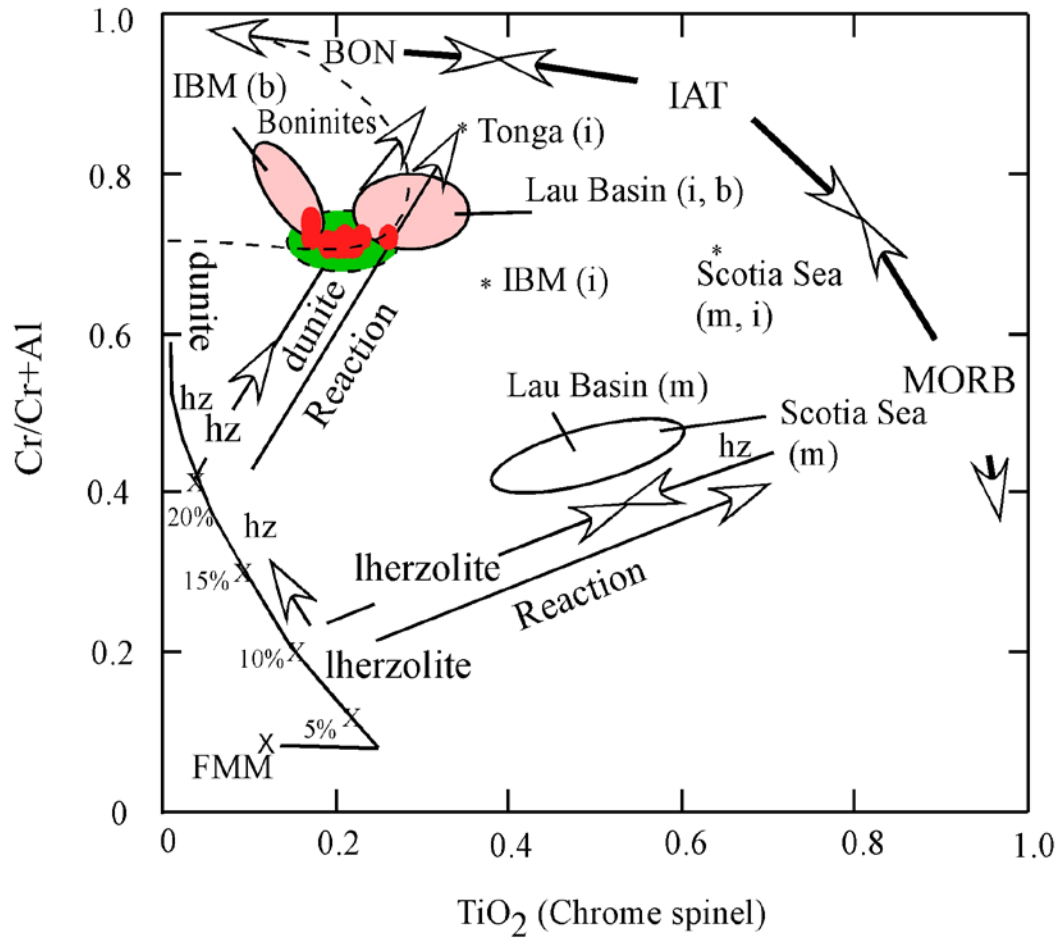


Figure 2.18. Cr# versus TiO_2 diagram for chromian spinel showing discrimination between partial melting trends and melt-mantle interaction trends (reproduced from Pearce et al., 2000; Sachan 2001; Khan et al., 2004). Abbreviations: I, b and m denote island arc tholeiite, boninite and MORB; IBM, Izu-Bonin-Mariana; FMM, fertile MORB mantle; BON, boninite.

2.7 Thermomagnetic analysis/isothermal remnant magnetization acquisition

The thermomagnetic analysis and isothermal remnant magnetization (IRM) acquisition experiment were also conducted on a magnetite grain in Geoscience Advance Research Laboratories, Islamabad. In the thermomagnetic analysis, the measurement was made for bulk sample using a horizontal curie balance Eiko/EB-4 under vacuum condition (Figs. 2.19, 2.20; Table 2.4). The thermomagnetic curve reveals reversible behavior with a single Curie temperature (585°C in heating curve and 595°C in cooling curve), which indicate single ferromagnetic phase similar to magnetite (Fe_3O_4). The Curie temperature is slightly higher than that of the synthetic pure magnetite (575°C to 580°C; Carmichael, 1989), which may be possibly due to some impurities in the magnetite crystal. Laboratory-induced isothermal remnant magnetization (IRM) in inductions up to 2.58T, were carried out by a 100ms-pulse magnetizer MMPM-9 (Magnetic Measurement Co). The IRM Acquisition/Demagnetization curves are shown in figure 2.20. Saturation of single domain (SD) magnetite normally requires inductions of as much as 250mT, whereas saturation of coarse-grained, multi-domain (MD) magnetite may occur in inductions of about 100mT (Dunlop, 1981). The result reveals that the IRM property of the opaque mineral is very similar to coarse-grained, MD magnetite. Very low remanence coercivity ($H_{cr} = 10\text{mT}$) also indicates MD state of the crystal.

Table 2.4. EPMA data of magnetite in peridot-bearing sheared dunite of the Sapat area.

Sample points	1	2	3	4	5	6	7	8	9
SiO ₂	0.087		0.074		0.007	0.033	0.072	0.026	0.211
TiO ₂		0.025			0.015	0.099			0.041
Al ₂ O ₃		0.021				0.01	0.039		
FeO	91.464	91.703	91.115	91.98	90.451	90.305	90.621	91.408	91.092
MnO	0.051	0.011	0.05	0.002	0.092	0.083		0.063	0.037
MgO	0.893	1.014	1.094	0.992	0.728	1.024	1.058	0.925	1.137
CaO									0.076
Na ₂ O	0.03	0.043	0.042	0.014	0.038	0.014	0.005	0.066	
K ₂ O		0.021	0.02			0.001		0.011	0.026
Cr ₂ O ₃	0.073	0.085	0.097		0.008	1.86	0.484	0.77	0.321
NiO	0.573	0.513	0.611	0.41	0.897	0.711	0.723	0.746	0.57
FeO	91.464	91.703	91.115	91.98	90.451	90.305	90.621	91.408	91.092

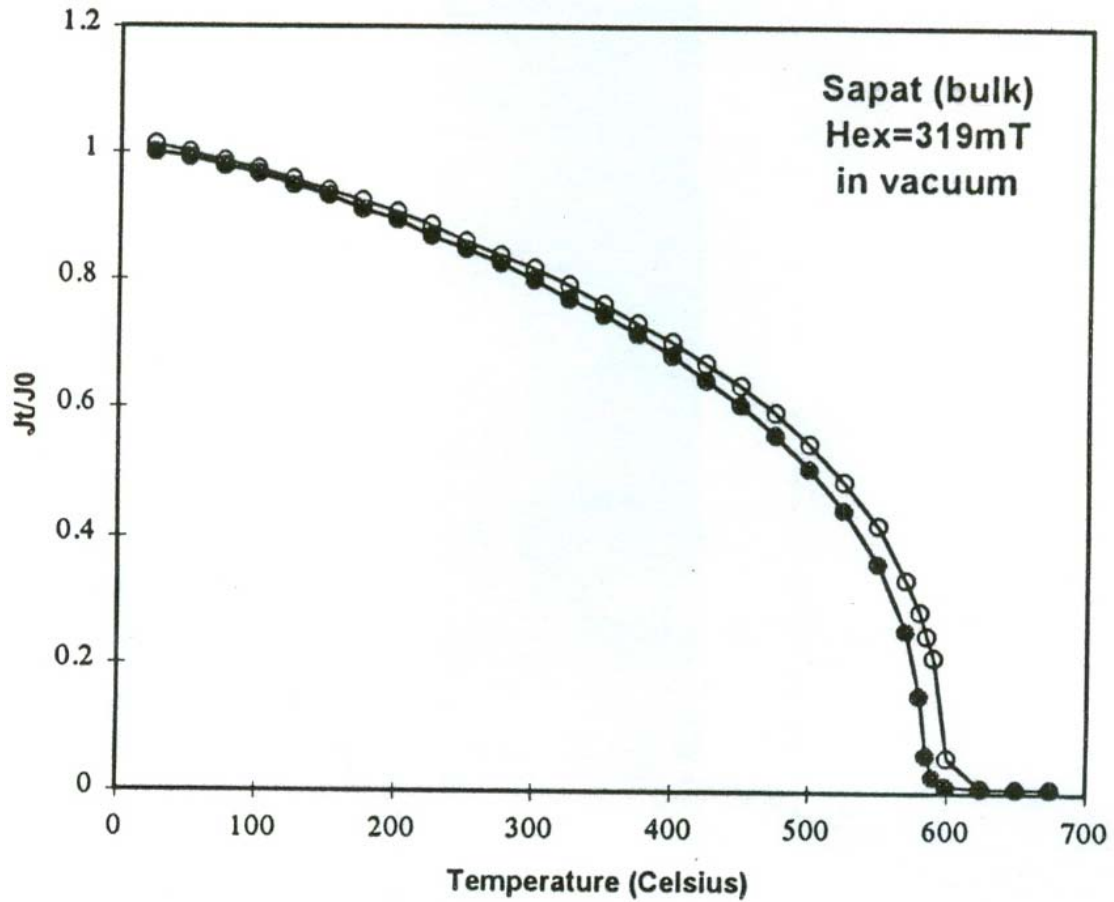


Figure 2.19. High-field (319mT) thermomagnetic curve of bulk mineral sample. Vertical axis is normalized by the initial (room temperature) magnetization ($=Jt/J0$). Closed circles indicate heating curve, open circles show cooling curve. The curve is clearly reversible which reveals a single phase ferromagnetic behavior. Curie temperature is determined at 585°C (in heating curve).

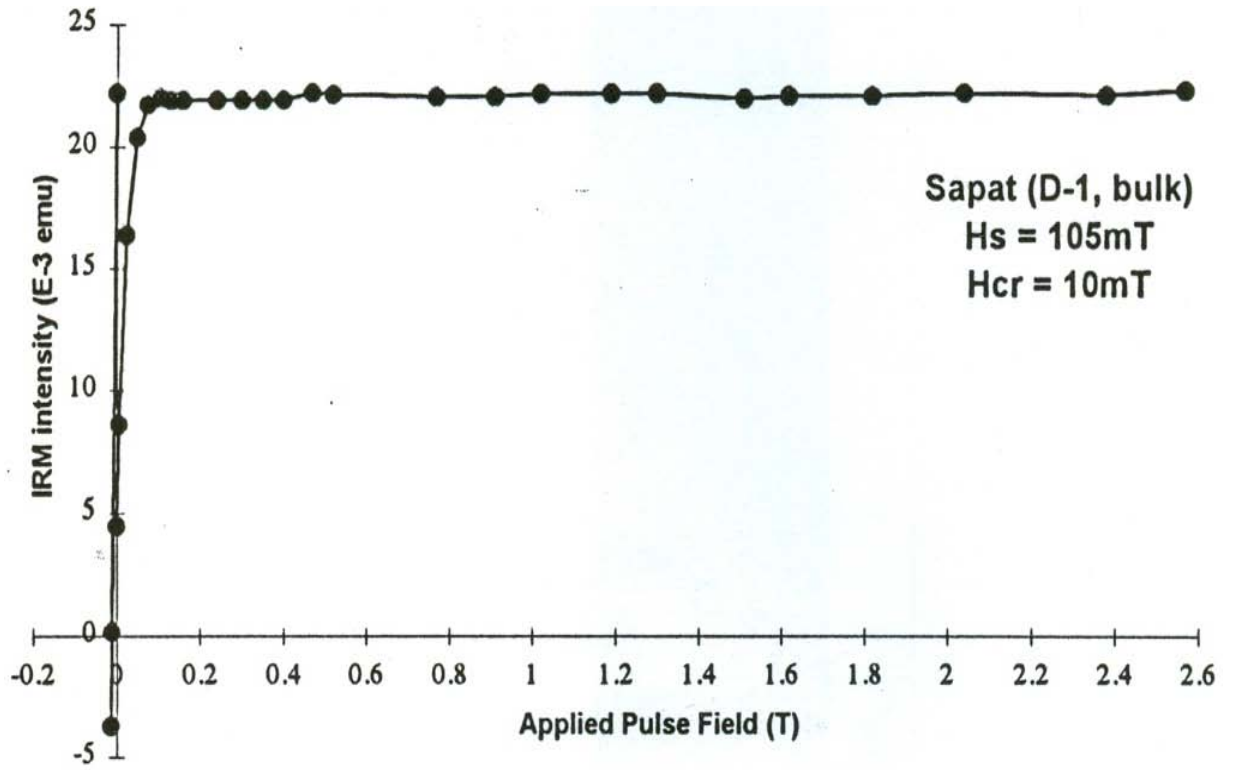


Figure 2.20. Laboratory induced isothermal remnant magnetization (IRM) acquisition/demagnetization curve of the bulk mineral sample at room temperature. The negative value of the applied field (H) shows the back-field demagnetization of saturated IRM by 2.56T. The saturation point (Hs) is around 105mT and the remnance coercivity (Hcr) determined by the back-field observation is -10mT.

2.8 Whole rock geochemistry

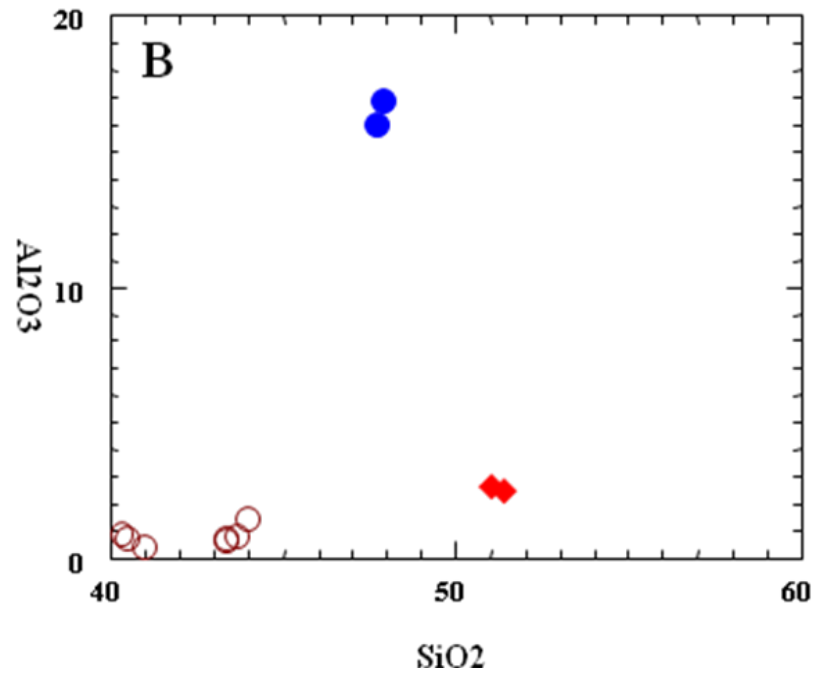
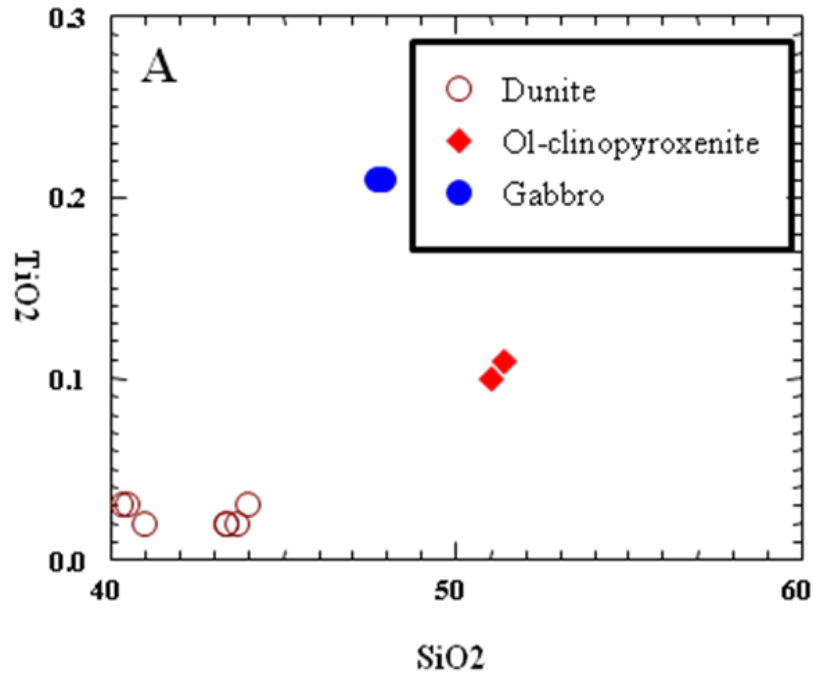
Analysis of 11 selected samples of ultramafic and gabbroic rocks from the Sapat complex are presented in Table 2.5. These data are used to decipher the range of internal variations in the studied rocks together with evaluation of their petrogenetic characteristics. A visible difference can be seen between the ultramafic and gabbroic rocks. The ultramafic rocks are typically rich in MgO, Ni and Cr relative to the gabbroic rocks. Dunite (SPT-4) stands distinct by the absence of CaO (<0.5 wt %) and highest MgO content (49.07 wt %). Al₂O₃ in this rock may be due to presence of spinel. The rest of analyzed ultramafic rocks contain variable proportions of CaO (4 to 20 wt %) depending upon the content of the clinopyroxene. Al₂O₃ content of all these rocks is less than 4 wt%, suggesting absence of cumulus plagioclase or amphibole. The gabbroic rocks by the presence of large amount of Al₂O₃ (>14 wt %) content depicts high proportions of plagioclase in gabbro of the area. Sample SPT-19 is the representative of peridot-bearing dunite.

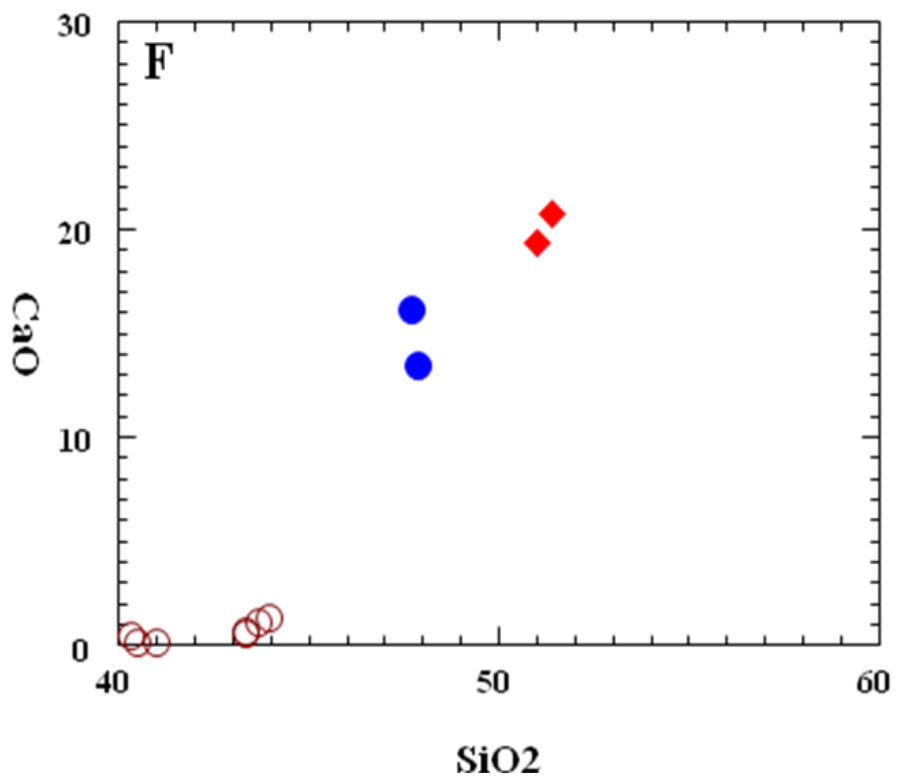
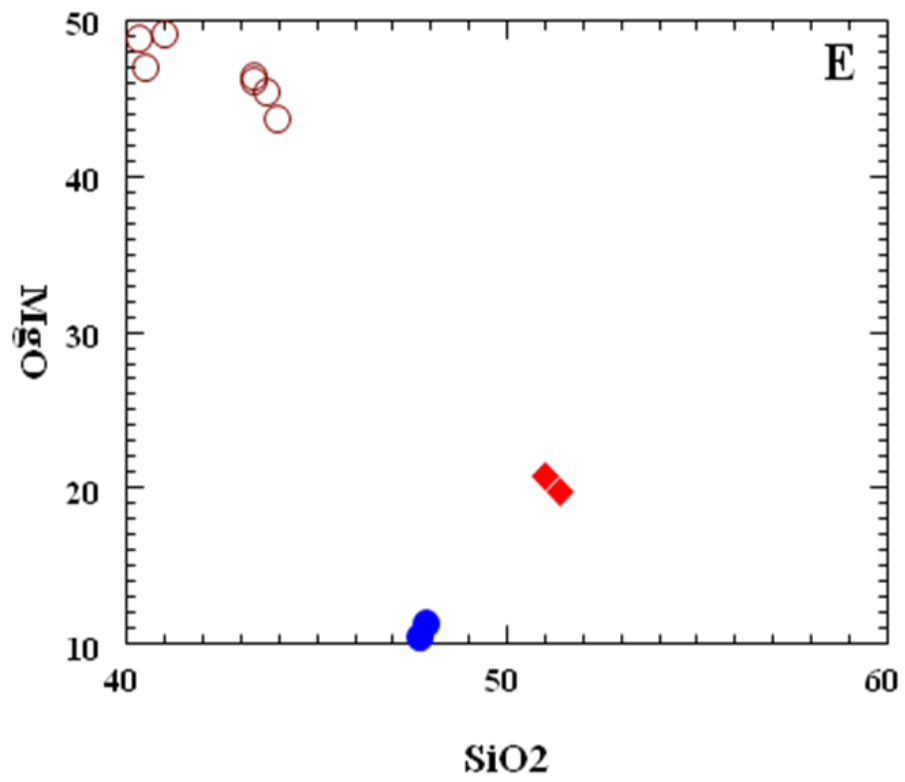
Table 2.5. Major and trace elements concentration (wt % and ppm) in the mafic and ultramafic rocks of the Sapat complex.

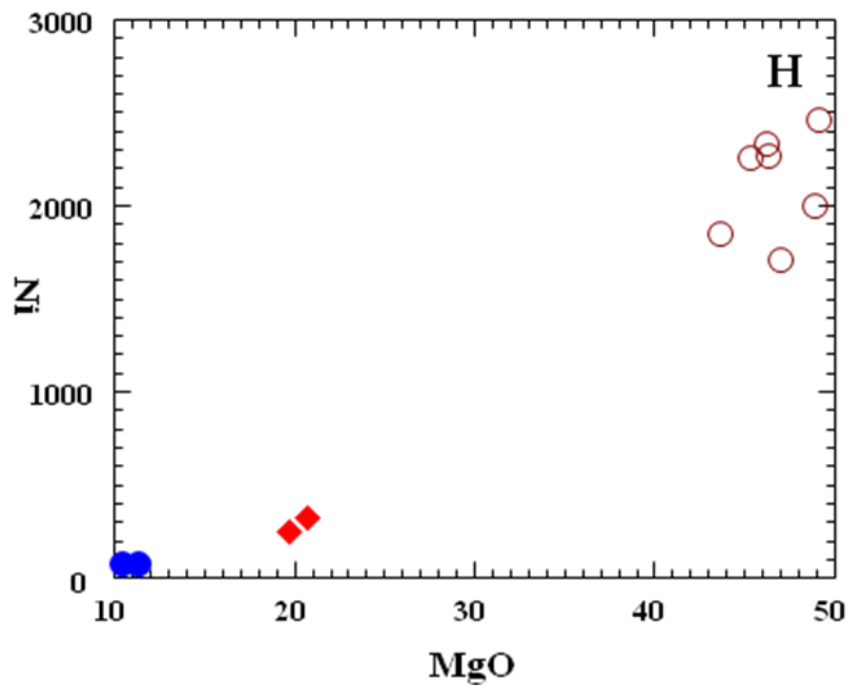
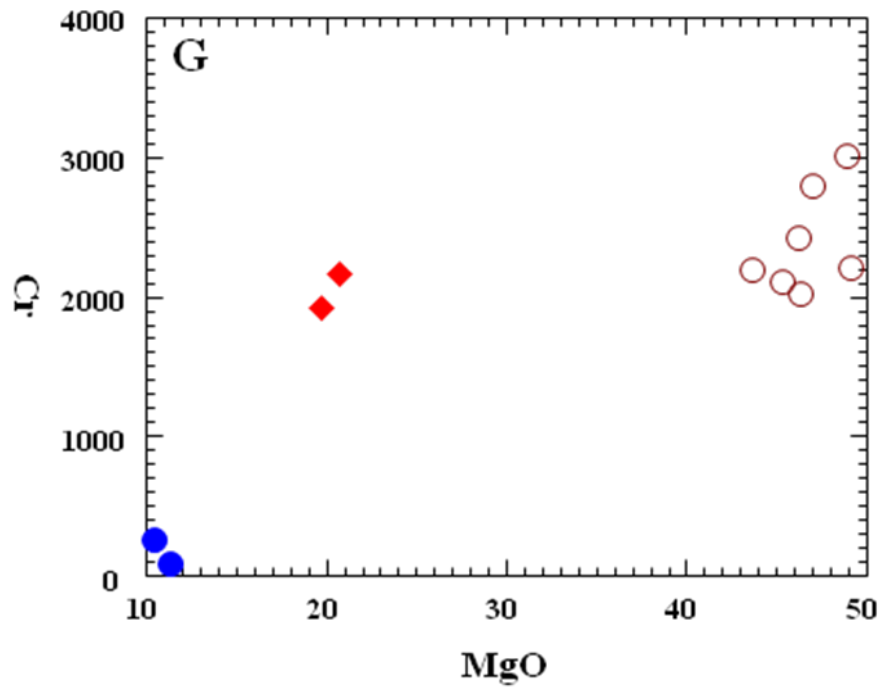
Sample	SPT2	SPT4	SPT5	SPT6	SPT7	SPT8	SPT11	SPT11A	SPT15	SPT17	SPT19
Rock	Dunite	Dunite	Dunite	Gabbro	Gabbro	Ol-clinopy.	Dunite	Ol-clinopy.	Dunite	Dunite	Dunite
SiO ₂	43.97	40.99	43.66	47.89	47.73	50.99	40.50	51.37	40.33	43.32	43.35
TiO ₂	0.03	0.02	0.02	0.21	0.21	0.10	0.03	0.11	0.03	0.02	0.02
Al ₂ O ₃	1.48	0.43	0.80	16.87	16.00	2.66	0.73	2.55	0.84	0.76	0.64
Fe ₂ O ₃	9.46	9.24	8.98	10.09	9.27	6.09	11.53	5.44	9.34	9.10	8.92
MnO	0.11	0.11	0.10	0.18	0.18	0.09	0.13	0.09	0.09	0.10	0.11
MgO	43.65	49.07	45.36	11.29	10.47	20.71	46.94	19.70	48.89	46.17	46.35
CaO	1.29	0.14	1.09	13.47	16.12	19.35	0.13	20.73	0.47	0.53	0.62
Y	6.00	6.00	6.00	7.00	7.00	7.00	6.00	7.00	6.00	6.00	6.00
V	18.00		7.00	181.00	254.00	172.00		185.00			
Cr	2196.00	2206.00	2106.00	95.00	264.00	2162.00	2798.00	1925.00	3015.00	2417.00	2023.00
Ni	1851.00	2459.00	2258.00	77.00	77.00	327.00	1712.00	244.00	2000.00	2335.00	2265.00
Co	141.00	159.00	147.00	61.00	55.00	100.00	151.00	79.00	169.00	147.00	148.00
Cu	20.00	24.00	11.00	103.00	58.00	165.00	12.00	78.00			
Zn	39.00	42.00	36.00	66.00	54.00	16.00	48.00	17.00	35.00	39.00	36.00
Mg#	0.92	0.93	0.92	0.72	0.73	0.89	0.91	0.89	0.92	0.92	0.92

Key: Ol-clinopy., Olivine clinopyroxenite.

Binary variation diagrams characterize these rocks to behave differently. These make 3 distinct groups when SiO₂ is used as fractionating index against other major and trace elements (Fig. 2.21A-J). Correlation coefficient is best illustrated in Mg# versus Al₂O₃ diagram (Fig. 2.22). Spider diagram used to illustrate trace elements patterns (Fig. 2.23). Dunite shows similar patterns but different from olivine clinopyroxenites and gabbros.







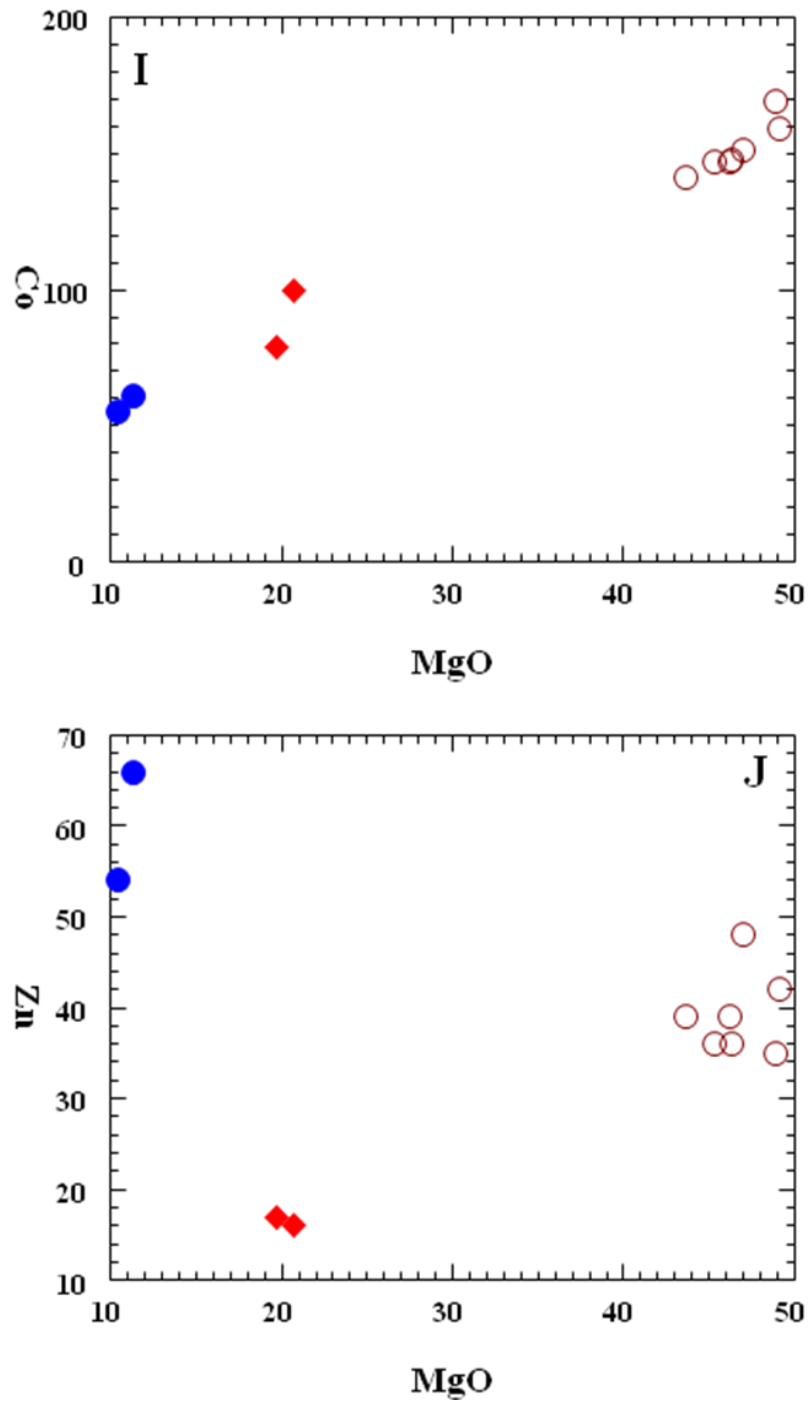


Figure 2.21. Plots illustrating SiO₂ as fractionating index for major elements and MgO for trace elements representing dunite, olivine clinopyroxenite and gabbro of the Sapat complex. Symbols for all the rocks are shown in the figure A. Symbol Ol stands for olivine.

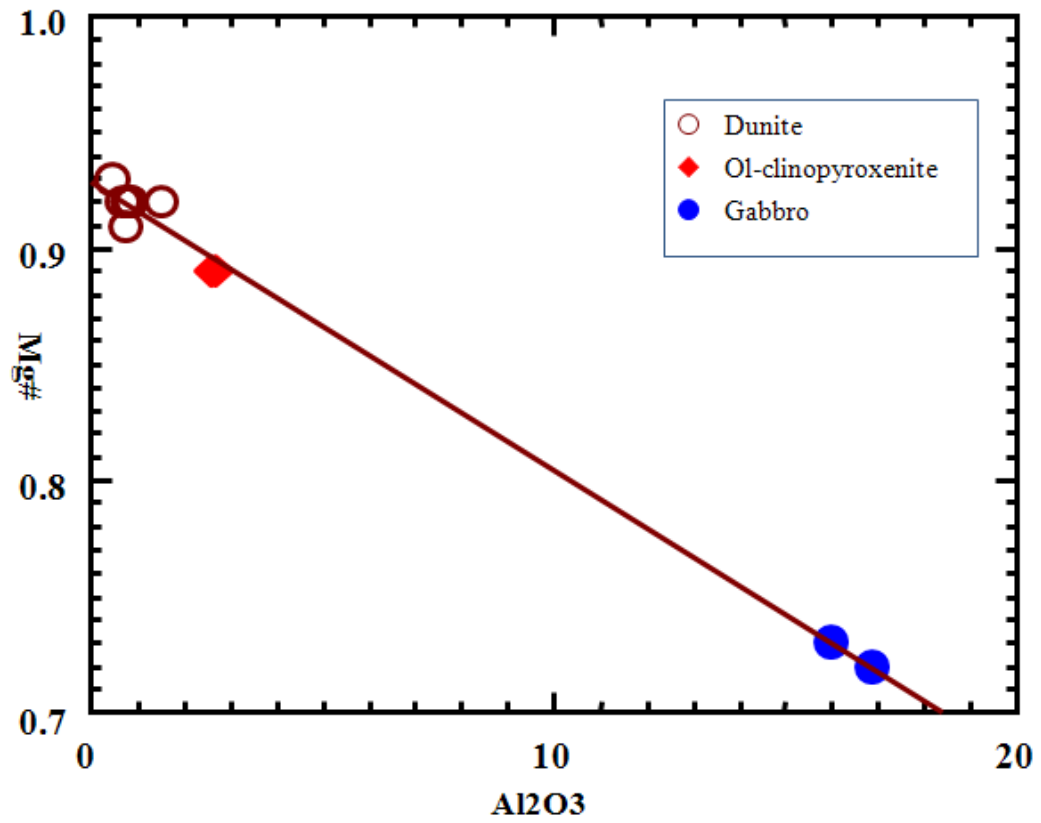


Figure 2.22. Mg# versus Al₂O₃ correlation coefficient variation diagram showing best fit regression line for the mafic and ultramafic rocks of the Sapat complex. Mg# is referred in table 3.5.

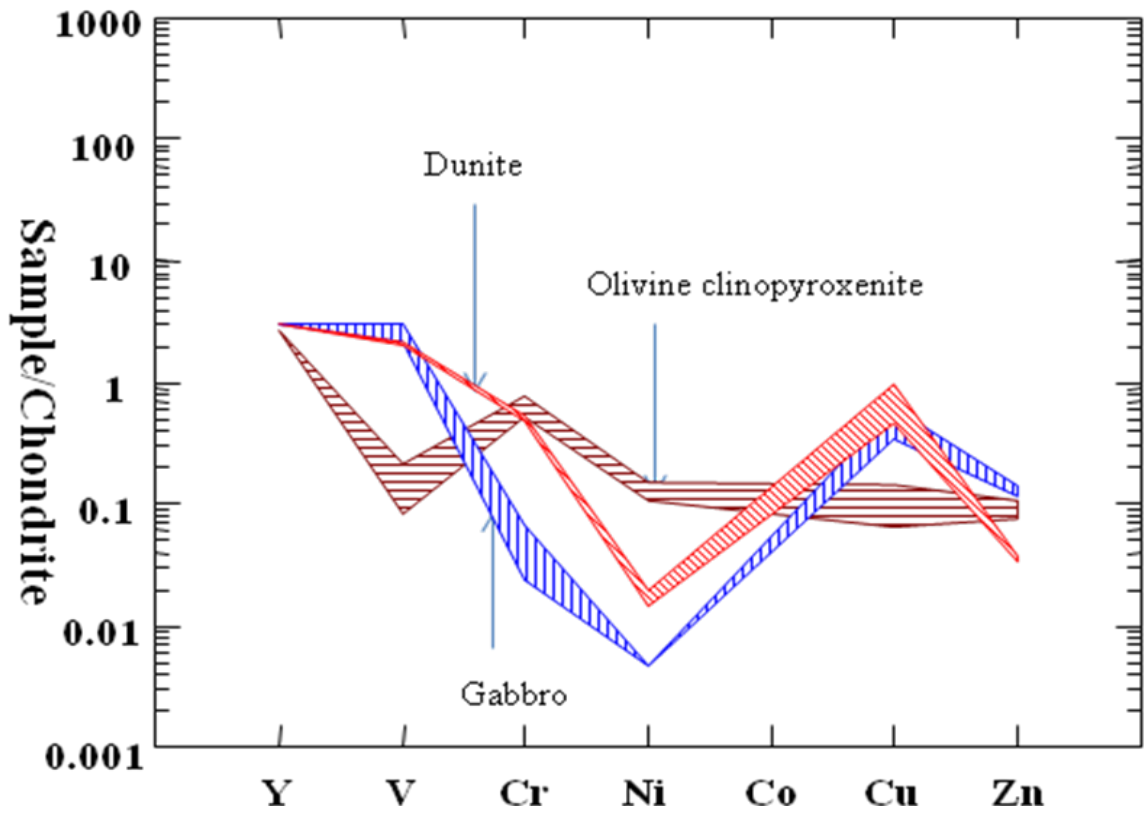


Figure 2.23. Chondrite normalized trace elements diagram for the dunite, olivine clinopyroxenite and gabbro of the Sapat complex. (Normalizing values are from Taylor and McLennan (1985).

DISCUSSION AND CONCLUSIONS

DISCUSSION

The Sapat complex of Jan et al. (1993) and/or Sapat peridotite of Bouilhol et al. (2009) occupies the same position (i.e. lying just immediate and above the MMT) in the Sapat area to that of the Jijal complex above the Besham dome in the Jijal area. Both the complexes have their lower contacts with the MMT and the upper contacts with the Kamila amphibolites (e.g. Bouilhol et al., 2009) and show almost similar lithological characteristics except local variations. For example the rocks in the Jijal complex are metamorphosed up to granulite facies and near to the contact with MMT ultramafics are metamorphosed into amphibolites (e.g. Sano et al., 1996). In the Sapat complex, the immediate rock at the contact with MMT is serpentized dunite, which is sheared and contains peridots.

Peridot mineralization has taken place in the joints/fissures and/or weak zones of the dunite. The mineralization is also accompanied with calcite, brucite, clinochrysotile and magnetite (e.g. Bouilhol et al., 2012). This activity normally takes place when the hydrothermal fluids pass through weak zone. The presence of ludwigite of Jan and Khan (1996) and Fe-Mg borate of Bouilhol et al. (2012) inclusions in peridot and peridot-calcite mineralization in weak zones, attest to the hydrothermal activity, probably resulted due to the processes in the mantle wedge (e.g. Bouilhol et al., 2012).

Petrographic study carried out on the peridot-bearing dunite, shows peridots to occupy the sheared parts of the rock. In relatively fresh part of dunite, clinochrysotile contains both olivine and peridot showing ribbon structure, which is due to deformation. The magnetite across the peridot grains may be due to deserpentinization (e.g. Deer et al., 1966). The Mg# variations against Al_2O_3 attest to one magma source for these rocks (Fig. 2.22). In spider diagram, dunites and pyroxenites show similar trend except that there is higher abundances of Ni and Cr in the dunite. The EPMA analyses of peridot show forsterite above 91 and a few up to 97 and 98. This enrichment of Mg may be from antigorite(?) Mg-Fe replacement can be seen in EPMA derived compositional image.

Based on this study and the research carried out by earlier workers, both metamorphism and hydrothermal activity may be the source of peridot mineralization.

The dunite in the Sapat and Jijal complexes (Fig. 1.1 inset), shows similarity in petrochemistry (e.g. Arif and Jan, 2006). The dunite of the Sapat complex does not contain any relict pyroxenes, however, the high Cr# >7.0 and the lower TiO₂ contents (0.18-0.27 wt. %) of the chromian spinel and the plotting of dunite within the olivine-spinel mantle array indicate its derivation from mantle (e.g. Arai, 1994). The NiO content of olivine in the dunite of the Sapat complex corresponds to lower values, may mean an involvement of orthopyroxene (Ni-poor) break down (e.g. Kelemen et al., 1998a). These data are consistent with formation of dunite by partial melting as according to Arai (1994), the OSMA is the residual peridotite array and the cumulates plot off this trend towards the fractional crystallization trend (Fig. 2.17). The data further shows inconsistency with formation of the dunite as olivine cumulates during fractional crystallization from primitive MORB (e.g. Depaolo 1981; Kelemen 1986; Navon and Stolper 1987; Keleman et al., 1998a) and plot in the overlapping field of island arc and boninites (Fig. 2.18). Based on Cr# >7.0 values in chromian spinel, it is inferred that the peridot-bearing dunite of the Sapat complex might have formed in the Kohistan forearc tectonic setting.

CONCLUSIONS

The following conclusions are derived from this research study:

1. The peridot mineralization in the deformed dunite seems to be due to hydrothermal activity and metamorphism.
2. The forsterite and nickel in olivine and Cr#, Al₂O₃ and TiO₂ in chromian spinel infer forearc tectonic setting for the origin of dunite.
3. Based on the correlation coefficients, the Sapat complex seems to be originated from single magma source.

REFERENCES

- Anczkiewicz, R., Oberli, F., Burg, J.P., Villa, I.M., Gunther, D. and Meier, M., 2001. Timing of normal faulting along the Indus Suture in Pakistan Himalaya and a case of major $^{231}\text{Pa}/^{235}\text{U}$ initial disequilibrium in zircon. *Earth and Planetary Science Letters* 191, 101-114.
- Arai, S., 1994. Characterization of spinel peridotites by olivine spinel compositional relationships: review and interpretation. *Chemical Geology* 113, 191-204.
- Arif, M. and Jan, M.Q., 2006. Petrotectonic significance of the chemistry of chromite in the ultramafic-mafic complexes of Pakistan. *Journal of Asian Earth Sciences* 27, 628-646.
- Bard, J.P., Maluski, H., Matte, P. and Proust, F., 1980. The Kohistan sequence: crust and mantle of an obducted island arc. *Geological Bulletin, University of Peshawar*, 13, 87-94.
- Bard, J.P., 1983. Metamorphism of an obducted island arc: Example of the Kohistan sequence (Pakistan) in the Himalayan collided range. *Earth and Planetary Science Letters* 65, 133-144.
- Bender, F.K. and Raza, H.A., 1995. *Geology of Pakistan. Betreige zur regionalen Geologie der Erde* 25. Gebruder Borntraeger, Berlin, 414p.
- Bouilhol, P., Burg, J.P., Bodinier, J.L., Schmidt, M.W., Dawood, H. and Hussain, S., 2009. Magma and fluid percolation in arc to fore- arc mantle: Evidence from Sapat Kohistan, Northern Pakistan. *Lithos* 1-2, 17-37.
- Bouilhol, P. and Burg, J.P., 2012. Gem olivine and calcite mineralization precipitated from subduction-derived fluids in the Kohistan arc-mantle. *The Canadian Mineralogist* 50, 1291-1304. DOI: 10.3749/canmin.50.5.1291.

- Burg, J.P., Bodinier, J.L., Chaudhry, S, Hussain, S. and Dawood, H., 1998. Infra-arc mantle-crust transition and intra-arc mantle diapers in the Kohistan complex (Pakistani Himalaya): petro-structural evidence. *Terra Nova* 10, 74-80.
- Carmichael, R.S., 1989. *Practical Hand Book of Physical Properties of Rocks and Minerals*. CRC Press, Boca Raton, 741p.
- Chaudhry, M.N., Kausar, A.B. and Lodhi, S.A.K., 1974. Geology of Timargara-Lal Qila area, Dir District, N.W.F.P. *Geological Bulletin, University of the Punjab* 11, 53-73.
- Chaudhry, M.N., Ghazanfar, M., Ashraf, M. and Shahid, S.S. 1984. Geology of Shewa-Dir-Yasin area and its plate tectonic interpretation. *Kashmir Journal of Geology* 2, 53-63.
- Coward, M.P., Windley, B.F., Broughton, R.D., Luff, I.W., Petterson, M.G., Pudsey, C.J., Rex, D.C. and Khan, M.A., 1986. Collision tectonics in the NW Himalayas In: Coward M.P., Ries A.C., (Eds.) *Collision Tectonics*. Geological Society of London Special Publication 19, 203-219.
- Coward, M.P., Butler, R.W.H., Khan, M.A. and Knipe, R.J., 1987. The tectonic history of Kohistan and its implications for Himalayan structure. *Geological Society of London* 144, 377-91.
- Deer, W.A., Howei, R.A. and Zussman, J., 1966. *An Introduction to the Rock forming Minerals*. Longman, London. Longman publisher, 528p.
- Depaolo, D.J., 1981. Trace elements and isotopic effects of combined wallrock assimilation and fractional crystallization. *Earth and Planetary Science Letters* 53, 189-202.
- Dick, H.J.B. and Bullen, T., 1984. Chromian spinel as a petrogenetic indicator in abyssal and alpine type peridotites and spatially associated lavas. *Contributions to Mineralogy and Petrology* 86, 54-76.

- Dunlop, J. D., 1981. The rock magnetism of fine particles. *Phy. Ear. Planet. Inter.*, 26, 1-26.
- Fleet, M.E., MacRae, N.D. and Herzberg, C.T., 1977. Partition of Nickel between olivine and sulfide: A test for immiscible sulfide liquids. *Contribution to Mineralogy and Petrology* 65, 191-198.
- Franz, L. and Wirth R., 2000. Spinel inclusions in olivine of peridotite xenoliths from TUBAF seamount (Bismarck Archipelago/Papua New Guinea): evidence from the thermal and tectonic evolution of the oceanic lithosphere. *Contributions to Mineralogy and Petrology* 140, 283-295.
- Ghazanfar, M., Chaudhry, M.N. and Hussain, M., 1991. Geology and petrotectonics of southeast Kohistan, northwest Himalaya, Pakistan. *Kashmir Journal of Geology* 8 and 9, 67-97.
- Honegger, K., Dietrich, V., Frank, W., Gansser, A., Thoni, M. and Trommsdorf, V., 1982. Magmatism and metamorphism in the Ladakh Himalaya (the Indus-Tsangpo suture zone). *Earth and Planetary Science Letters* 60, 253-292.
- Hussain, S.S., 2005. Geology of the Indus Suture Zone and High Himalayan Crystalline Block west of Besham syntaxis and study of some associated minerals. Institute of Geology, University of the Punjab, Lahore, PhD thesis, 79-81p.
- Jan, M.Q., 1977. The Kohistan basic complex: A summary based on recent petrological research. *Geological Bulletin, University of Peshawar* 9 and 10, 36-42.
- Jan, M.Q., 1979. Petrography of pyroxene granulites from northern Swat and Kohistan. *Geological Bulletin, University of Peshawar, Special Issue* 11, 65-87.
- Jan, M.Q. and Howie, R.A., 1981. The mineralogy and geochemistry of the metamorphosed basic and ultrabasic rocks of the Jijal complex, Kohistan, NW Pakistan. *Journal of Petrology* 22, 85-126.

- Jan, M.Q. and Windley, B.F., 1990. Chromian spinel-silicate chemistry in ultramafic rocks of the Jijal complex, NW Pakistan. *Journal of Petrology* 31 (3), 667-715.
- Jan, M.Q., Khan, M.A. and Qazi, M.S., 1993. The Sapat mafic-ultramafic complex, Kohistan arc, North Pakistan. *Geological Society of London, Special Publication* 74: 113-121.
- Jan, M.Q. and Khan, A., 1996. Petrology of gem peridot from Sapat mafic-Ultramafic complex, Kohistan, NW Himalaya. *Geological Bulletin, University of Peshawar* 29, 17-26.
- Kausar, A.B. and Khan, T., 1996. Peridot mineralization in the Sapat ultramafic sequence, Naran- Kohistan Pakistan. *Geologica* 2, 69-75.
- Kazmi, A.H., Lawrence, R.D., Dawood, H., Snee, L.W. and Hussain, S.S., 1984. Geology of the Indus Suture Zone in the Mingora-Shangla area of Swat, North Pakistan. *Geological Bulletin, University of Peshawar* 17, 127-144.
- Kazmi, A.H. and O'Donoghue, M., 1990. *Gemstones of Pakistan*. Gemstone Corporation of Pakistan, 146p.
- Kazmi, A.H. and Jan, M.Q., 1997. *Geology and tectonics of Pakistan*. Graphic publishers, Pakistan, 554p.
- Kelemen, P.B., 1986. Assimilation of ultramafic rocks in the subduction related magmatic arcs. *Journal of Geology* 94, 829-843.
- Kelemen, P.B., Hart, S.R. and Bernstein, S., 1998a. Silica enrichment in the continental upper mantle via melt/rock reaction. *Earth and Planetary Science Letters* 164, 387-406.
- Keller, C.P., 1990. *Gemstones and their origin*. Van Nostrand Reifold Publishers, New York, 144p.

- Khan, M.A., Jan, M.Q., Windley, B.F., Tarney, J. and Thirwall, M.F., 1989. The Chilas mafic ultramafic igneous complex: The roots of the Kohistan island arc in the Himalaya of northern Pakistan. In: Tectonics of the western Himalayas. Malinconico, L. L. and Lillie, R.J. (Eds.). Geological Society of America Special Paper (232), 75-94.
- Khan, M.A., Jan, M.Q. and Weaver, B.L., 1993. Evolution of the lower arc crust in Kohistan, N. Pakistan: Temporal arc magmatism through early mature and intra-arc rift stages. In: Himalayan Tectonics. In: Treloar, P.J. and Searle, M.P. (Eds.). Geological Society of London Special Publication 74, 123-128.
- Khan, M.A., Jan, M.Q., Qazi, M.S., Khan, M. Ahmad., Shah, Y. and Sajjad, A., 1995. Geology of the drainage divide between Kohistan and Kaghan, N. Pakistan. Geological Bulletin University of Peshawar 28, 65-77.
- Khan, S.D., Walker, D.J., Hall, S.A., Burkek, C., Shah, M.T. and Stockli, L., 2009. Did the Kohistan- Ladakh island arc collide first with India? Geological Society of America Bulletin 121, 366-84.
- Khan, T., 1994. Evolution of the Upper and Middle Crust in Kohistan Island Arc, North Pakistan. PhD thesis, National Centre of Excellence in Geology, University of Peshawar, Peshawar, 225p.
- Khan, T., Khan, M. A. and Jan, M. Q., 1994. Geology of a part of the Kohistan terrain between Gilgit and Chilas, northern areas, Pakistan. Geological Bulletin, University of Peshawar 27, 99-112.
- Khan, T., Jan, M.Q., Khan, M.A. and Latif, M., 1996. Geology of a part of the Kohistan terrane between Gilgit and Chilas, North Pakistan: Regional tectonic implications. Journal of Nepal Geological Society 14 Special Issue, 1-10.
- Khan, T., Khan, M.A., Jan, M.Q. and Naseem, M., 1996. Back-arc basin assemblages in Kohistan, Himalaya, N. Pakistan. Geodynamica Acta (Paris) 9, 30-40.

- Khan, T., Kausar, A.B. and Khan, I.H., 1997. Peridot mineralization in the Sapat ultramafic sequence of the Indus Suture Zone, Naran-Kohistan area, northern Pakistan. Abstract: 12th Himalaya-Karakoram-Tibet International Workshop, Rome, Italy, 159-164.
- Khan, T., Kausar, A.B. and Khan, I.H., 2000. Mantle Thrust Sheet Peridot Deposits: An Example from Sapat, Naran-Kohistan Areas, Himalaya, Pakistan. Abstract: 1st International Gems and Minerals Conference, Peshawar, Pakistan.
- Khan, T., Murata, M., Ozawa, H. and Kausar, A.B., 2004. Origin of dunite of the Sapat Complex, Himalaya, North Pakistan. Extended Abstract: Himalayan Journal of Sciences 2 (4) Special Issue, p.179.
- Khan, T., Murata, M., Karim, T., Zafar, M., Ozawa, H. and Rehman, H., 2007. A Cretaceous dike swarm provides evidence of a spreading axis in the back-arc basin of the Kohistan paleo-island arc, northwestern Himalaya, Pakistan. Journal of Asian Earth Sciences 29, 350-360.
- Khan, T. and Kausar, A.B., 2010. Gems and Gemology in Pakistan. Geological Survey of Pakistan Special Publication, 231p.
- Khan, T., Murata, M., Zafar, M. and Rehman, H., 2011. Petrogenetic comparison of the mafic dykes in the Kohistan paleo-island arc-back-arc system, Himalayas of North Pakistan. In: Rajesh K. Srivastava (Eds.) Dyke Swarms: Keys for Geodynamic Interpretation, Springer, 437-455.
- Koivula, R.C., Kammerling, R.C. and Fritsch, E., 1994. Gem News. Gems and Gemology 30, 191-201 and 271-280.
- Miller, D.J., Loucks, R.R. and Ashraf, M., 1991. Platinum group elements mineralization in the Jijal layered mafic-ultramafic complex, Pakistani Himalayas. Economic Geology 86, 1093-1102.

- Navon, O. and Stolper, E., 1987. Geochemical consequences of melt percolation: the upper mantle as a chromatographic column. *Journal of Geology* 95, 285-307.
- Pearce, J.A., Barker, P.F., Edwards, S.J., Parkinson, J.I. and Leat, P.T., 2000. Geochemistry and tectonic significance of peridotites from the South Sandwich arc-basin system, South Atlantic. *Contribution to Mineralogy and Petrology* 139, 36-53.
- Petterson, M.G. and Windley, B.F., 1985. Rb-Sr dating of the Kohistan arc batholiths in the Transhimalayan of the North Pakistan and tectonic implications. *Earth Planetary Science Letters* 74. 45-57.
- Rehman, H., Seno, T., Yamamoto, H. and Khan, T., 2011. Timing of collision of the Kohistan- Ladakh with India and Asia, *Island Arc* 20,308-328p.
- Ringuette, L., Martignole, J. and Windley, B.F., 1998. Pressure-Temperature evolution of garnet bearing rocks from the Jijal complex, (western Himalayas, northern Pakistan): from High-pressure cooling to decompression and hydration of a magmatic arc. In: Hamidullah, S., Lawrence, R.D. and Jan, M.Q. (Eds.) Abstract: 13th Himalaya-Karakoram- Tibet International Workshop, *Geological Bulletin, University of Peshawar* 31, 167-168.
- Sachan, H.K., 2001. Supra-subduction origin of the Nidar ophiolite sequence, Indus Suture Zone, Ladakh, India: evidence from mineral chemistry of upper mantle rocks. *Ophioliti* 26 (1), 23-32.
- Sano, S., Nakajima, T. and Khan, S.R., 1996. Geology and isotope geochemistry of the Jijal complex, Kohistan, northern Pakistan. *Proceedings of. Geoscience Colloquium* 15, 127-135.
- Schaltegger, U., Zeilinger, G., Frank, M. and Burg, J.P., 2002. Multiple mantle sources during island arc magmatism: U- Pb and Hf isotopic evidence from the Kohistan arc complex, Pakistan. *Terra Nova* 14, 461-468.

- Shams, F.A., Jones, G.C. and Kempe, D.R.C., 1980. Blueschists from Topsis, Swat District, NW Pakistan. *Mineralogical Magazine* 43, 941-942.
- Sullivan, M.A., Windley, B.F., Saunders, A.D., Haynes, J.R. and Rex, D.C., 1993. A palaeogeographic reconstruction of the Dir Group: evidence for magmatic arc migration within Kohistan, N. Pakistan. In: Treloar, P.J. and Searle, M.P. (Eds.) *Himalayan tectonics. Geological Society of London Special Publication* 74, 139-160.
- Tahirkheli, R.A.K., Mattauer, M., Proust, F. and Tapponnier, P., 1979. The India-Eurasia suture zone in northern Pakistan: Synthesis and interpretation of data at plate scale. In: Farah, A. and Dejong, K. (Eds.) *Geodynamics of Pakistan. Geological Survey of Pakistan, Monograph*, 125-130.
- Tahirkheli, R.A.K., 1982, *Geology of the Himalaya, Karakoram and Hindukush in Pakistan. Geological Bulletin, University of Peshawar* 15, 1-51.
- Taylor, S.R. and McLennan, S.M., 1985. *The Continental Crust: Its Composition and Evolution. Blackwell, Oxford*, 275-282.
- Treloar, P.J., Petterson, M.G., Jan, M.Q. and Sullivan, M.A., 1996. A re-evaluation of the stratigraphy and evolution of the Kohistan arc sequence, Pakistan Himalaya: Implications for magmatic and tectonic arc-building processes. *Geological Society of London* 153, 681-93.
- Yamamoto, H and Nakamura, E., 2000. Timing of magmatic and metamorphic events in the Jijal complex of Kohistan arc deduced from Sm-Nd dating of mafic granulites. In Khan, M.A., Treloar, P.J., Searle, M.P. and Jan, M.Q. (Eds.) *Tectonics of the Nanga Parbat Syntaxis and the Western Himalaya. Geological Society of London Special Publication* 170, 313-19.

Internet Links

<http://semiprecious.com>

[http://www.pakwheels.com/forums/road-trips-vacations/104142-kaghan-valley-sapat-souch village-naran-kaghan](http://www.pakwheels.com/forums/road-trips-vacations/104142-kaghan-valley-sapat-souch-village-naran-kaghan)

http://www.pakistanpaedia.com/land/kaghan/valleys-of-pakistan_kaghan.html

http://en.wikipedia.org/wiki/Kaghan_Valley

<http://pr.hec.gov.pk/Chapters/2760H-3.pdf>